Phase transitions and minimal interfaces on manifolds with conical singularities

March 11, 2024

Daniel Grieser*, Sina Held†, Hannes Uecker‡ and Boris Vertman♯

Abstract

Using Γ–convergence, we study the Cahn-Hilliard problem with interface width parameter $\varepsilon>0$ for phase transitions on manifolds with conical singularities. We prove that minimizers of the corresponding energy functional exist and converge, as $\varepsilon\to 0$, to a function that takes only two values with an interface along a hypersurface that has minimal area among those satisfying a volume constraint. In a numerical example, we use continuation and bifurcation methods to study families of critical points at small $\varepsilon>0$ on 2D elliptical cones, parameterized by height and ellipticity of the base. Some of these critical points are minimizers with interfaces crossing the cone tip. On the other hand, we prove that interfaces which are minimizers of the perimeter functional, corresponding to $\varepsilon=0$, never pass through the cone tip for general cones with angle less than 2π. Thus tip minimizers for finite $\varepsilon>0$ must become saddles as $\varepsilon\to 0$, and we numerically identify the associated bifurcation, finding a delicate interplay of $\varepsilon>0$ and the cone parameters in our example.

Contents

1 Introduction and statement of the main results 1
2 Convergence of minimizers on singular spaces 6
3 Minimizers on cones in 2D: interfaces 15
4 Minimizers on cones: Numerical illustrations 17
A Appendix: Auxiliary aspects of geometric measure theory 27
B Conical singularities. $\mathcal{D}(\Delta_D), \mathcal{D}(\Delta_N)$ versus $H^2(M)$ 31

1. Introduction and statement of the main results

1.1. The Cahn-Hilliard problem.

In the Cahn-Hilliard gradient theory of phase transitions we are interested in the minimizers, or more generally critical points, of the energy functional

$$E_\varepsilon(u) := \frac{1}{2\sigma}\int_M \frac{\varepsilon}{2}|\nabla u|_g^2 + \frac{1}{\varepsilon}W(u)\,\mathrm{dvol}_g, \qquad (1.1)$$

where $\varepsilon > 0$ is a parameter, (M, g) is a possibly incomplete Riemannian manifold of dimension d, of finite volume $\mathrm{vol}_g(M)$, with boundary ∂M, and we have used the notation W for a *double well potential*, e.g. $W(x) := \frac{1}{4}(x^2 - 1)^2$ for $x \in \mathbb{R}$ (this can be replaced by any coercive C^1 function with exactly two minima), and the normalization

$$\sigma := \int_{-1}^{1} \sqrt{W(x)/2}\, dx = \frac{\sqrt{2}}{3}.$$

We minimize among real-valued $u \in H^1(M) \cap L^4(M)$, subject to Neumann boundary conditions $\partial_\nu u{=}0$ on the boundary ∂M (with normal unit vector field ν) and under the mass constraint

$$\langle u \rangle := \frac{1}{\mathrm{vol}_g(M)} \int_M u \, d\mathrm{vol}_g = m, \tag{1.2}$$

where $m \in [-1, 1]$ is a *prescribed mass*, often set to $m = 0$ below. Using the Lagrange multiplier λ we introduce the Lagrangian

$$L(u, \lambda) = E_\varepsilon(u) + \lambda\Big(\langle u \rangle - m\Big). \tag{1.3}$$

Then the first variations of $L(u, \lambda)$ with respect to u and λ yield the Euler–Lagrange equations as necessary first order minimization conditions,

$$\begin{aligned} &\text{(a)} \quad -\varepsilon^2 \Delta u + W'(u) - \lambda = 0 \text{ in } M, \quad \partial_\nu u = 0 \text{ on } \partial M, \\ &\text{(b)} \quad q(u) = 0, \qquad \text{where } q(u) := \langle u \rangle - m, \end{aligned} \tag{1.4}$$

where Δ is the (negative) Laplace–Beltrami operator associated to (M, g). The PDE (a) with $\lambda = 0$ is also called Allen–Cahn equation. The trivial (spatially homogeneous) solution branch of (1.4) is $u \equiv m$, with Lagrange multiplier $\lambda = W'(m)$.

1.2. **Relation to minimal hypersurfaces.** The problem (1.1) is closely related to constant mean curvature surfaces in M, i.e. surfaces which have minimal area among those satisfying a volume constraint. The pure phases $u = \pm 1$ minimize the double well potential W and hence also the energy functional E_ε with the mass constraint $m = \pm 1$, respectively. However, for $|m| \neq 1$ these minimizers do not fulfill the mass constraint (1.4b), and instead we expect regions of pure phases $u = 1$ and $u = -1$ separated by transition regions or interfaces with $u \in (-1, 1)$. The term $\frac{\varepsilon}{2}|\nabla u|_g^2$ models an interface energy density, and for $\varepsilon > 0$ the minimizers u_ε are smooth. However, from the ε–scaling together with the scaling of the potential energy $\frac{1}{\varepsilon}W(u)$ we expect the interfaces to be steep and of width $\mathcal{O}(\varepsilon)$. This suggests that suitable sequences of minimizers u_ε of E_ε for $\varepsilon \to 0$ converge to a function u_0 which only takes values in the *pure phases* $u = \pm 1$, and such that the interface

$$I_0 = \partial\{u_0 {=} -1\} \subset M \backslash \partial M \tag{1.5}$$

(we take the boundary in $M \setminus \partial M$, so that ∂M is not part of the interface) has minimal $(d-1)$-dimensional volume among those satisfying the mass constraint (1.4)(b).[1]

The above heuristics is proven in [Mod87] for domains in Euclidean space, with the following precise statement where henceforth we write

- *length* for the $(d-1)$-dimensional volume,
- *area* for the d-dimensional volume.

Theorem 1.1. *Let $\Omega \subset \mathbb{R}^d$ be a bounded domain with Lipschitz boundary. Let (u_ε) be a sequence of minimizers of E_ε with $\varepsilon \to 0$, subject to $q(u_\varepsilon) = 0$ with $|m| < 1$. Then there exists a subsequence of (u_ε) that converges in $L^1(\Omega)$ to a function u_0 which only takes values in ± 1, with the interface I_0 as in (1.5) having minimal length $|I_0|$ among those satisfying the mass constraint. Moreover, for that subsequence*

$$\lim_{\varepsilon \to 0} E_\varepsilon(u_\varepsilon) = |I_0|.$$

Results of this type have been extended and refined, and have been transferred to Cahn–Hilliard problems on (smooth) Riemannian manifolds, including min–max type results for critical points of E_ε (saddle–points), see, e.g., [GHP03, Ton05, Pac12, GG18, BNAP22, HT00]. A standard setting for this is Γ–convergence, already discussed in [Mod87], see [Rin18, §13] for a textbook presentation.

1.3. **Main results: a) Convergence of minimizers.** Our first main result is the transfer of the convergence of minimizers results as in Theorem 1.1 to the case of compact manifolds with boundary and conical singularities, using results from geometric measure theory [Mor16, Fed14]. These spaces, denoted $\overline{M}$, with regular part the Riemannian manifold (M, g), are defined in Appendix B, and we show as a combination of Propositions 2.2, 2.3 and Theorem 2.5 the following. As before, we fix a mass satisfying $|m| < 1$.

Theorem 1.2. *Let $\overline{M}$ be a compact manifold with boundary and finitely many conical singularities. Then the following holds*

1. *Minimizers u_ε of E_ε with $q(u_\varepsilon) = 0$ and satisfying Neumann boundary conditions at ∂M exist for $\varepsilon > 0$ and are strong solutions to the Allen-Cahn equation (1.4).*

2. *E_ε Γ-converges to E_0 as $\varepsilon \to 0^+$ with respect to the strong L^1-topology, where E_0 is the perimeter functional, see (2.19) for the precise definition. In particular, if (u_ε) is a sequence of such minimizers for $\varepsilon \to 0$, and $u_\varepsilon \to u_0$ in $L^1(M)$, then u_0 only takes values in ± 1, the interface I_0 as in (1.5) has minimal length $|I_0|$ among the hypersurfaces satisfying the mass constraint, and*

$$\lim_{\varepsilon \to 0} E_\varepsilon(u_\varepsilon) = |I_0|. \tag{1.6}$$

[1] The mass constraint amounts to $\frac{\mathrm{vol}\{u=1\}}{\mathrm{vol}\{u=-1\}} = \frac{1+m}{1-m}$ for $|m| < 1$.

Remark 1.3. a) The convergence of a subsequence $u_\varepsilon \to u_0$ in $L^1(M)$ can be obtained under rather general conditions, see [Mod87, Proposition 3] for the Euclidean case, namely if (a) $(u_\varepsilon(x))$ is bounded in L^∞, or (b) under natural growth conditions for W, for instance fulfilled by our prototype W. The proof from [Mod87] transfers directly to manifolds as in Thm 1.2, and similar for a proof of (a) from [GM88] under different assumptions on W. Thus, in Theorem 1.2 we mainly assume $u_\varepsilon \to u_0$ in $L^1(M)$ for simplicity.

b) In the smooth case (1.6) is obtained in [GG18] also for sequences u_ε which have Morse index $\mathrm{ind}(u_\varepsilon) = 1$ for all ε, i.e., saddle points of the energy.

1.4. **Main results: b) Minimizers on conical surfaces.** Our second main result studies minimizers of E_0 on surfaces with boundary and conical singularities, namely in Proposition 3.2 we prove the following. See Appendix B for the definition of the angle of a conical singularity.

Proposition 1.4. *Let $\overline{M}$ be a surface with boundary and a conical singularity P of angle $\alpha < 2\pi$. Then any curve of minimal length which divides $\overline{M}$ into two parts of prescribed area ratio does not pass through P.*

1.5. **Main results: c) Numerical study of minimizers.** Our third contribution is a numerical study of critical points of E_ε on 2D cones, see Fig. 1 for a preview of "typical" solutions on a "typical" cone at ε=0.1. Here we restrict to $m = 0$. Numerically, the problem is best considered by continuation and bifurcation: we first fix $\varepsilon > 0$ and aim to obtain a selection of solutions u_ε at $m = 0$, by bifurcation of nonhomogeneous solutions u_ε from the homogeneous branch $u \equiv m$ and continuation to $m = 0$. Subsequently, we consider continuation in $\varepsilon \to 0$, aiming to identify the limiting interfaces I_0, and to check the formula (1.6).[2]

In addition to the parameters m and ε, in our numerics we consider elliptic cones of height $h > 0$ with short semi-axis 1 and long semi-axis $a \geq 1$. This yields rather rich bifurcation diagrams and different types of interfaces as seen in the numerical examples in Fig. 1.

1. ***Type T1 interfaces*** **passing through the conical tip ('tip-interfaces'):**

   We find that for any $\varepsilon > 0$ and $h > 0$ there is a (large) $a_0 \geq 1$ such that for all $a > a_0$ the minimizer of E_ε shows an interface going through the tip of the cone along the short semi–axis, i.e., of length $2\sqrt{1 + h^2}$. For instance Fig. 1(a), at fixed $\varepsilon = 0.1$, shows such a tip–interface u_ε with $\mathrm{ind}(u_\varepsilon) = 1$, i.e., a saddle point for E_ε (since $a = 1.05$ is small here).

2. ***Type T2 interfaces*** **winding around the conical tip:**

   Fig. 1 (b) shows a local (and global) minimizer of type T2.

[2] A similar numerical analysis is performed e.g. in [Uec21, §6.9 and §10.1] over 2D and 3D flat and curved (non-singular) manifolds, also including the case of finite Morse index saddle points, for which we numerically obtain the same convergence as for mininizers as in Theorem 1.1, see also Remark 1.3(b).

(a) T1 (b) T2 (c) T3

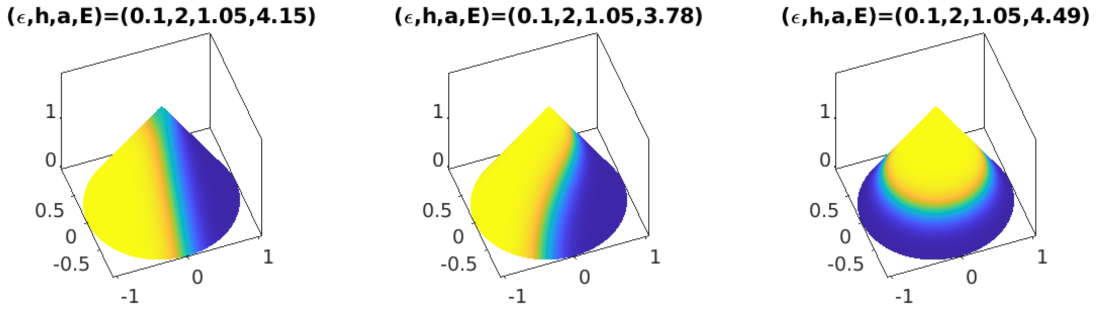

Figure 1: Three basic types T1, T2 and T3 of interfaces on a cone of height $h = 2$, ellipticity $a = 1.05$ (almost circular); $\varepsilon = 0.1$, energy $E = E_\varepsilon$ as given, approximating the interface length. The *tip interface* T1 is a saddle point here (but for fixed small $\varepsilon > 0$ becomes a global minimizer on a sufficiently elliptic cone); T2 (winding) is the global minimizer, and T3 (roughly horizontal) is a local minimizer; see §4 for details.

3. ***Type T3 interfaces* running horizontally around the tip:**

   Fig. 1 (c) shows another saddle point of type T3 with a roughly "horizontal" interface, and we expect T3 solutions to become minimizers at large h (for small $\varepsilon > 0$, and also in the limit $\varepsilon \to 0$).

In §4 we present the numerical computations partly previewed in Fig.1. Naturally, the limit $\varepsilon \to 0$ is of particular interest for sequences of tip–interfaces, while for (sequences of) interfaces which avoid the tip as in Fig. 1(b,c) we are essentially back to the non–singular case.

The angles of our elliptic cones are always less than 2π, so tip–interfaces are *never* minimizers at $\varepsilon = 0$ by Proposition 1.4. Therefore, in the numerical continuation in $\varepsilon \to 0$ for T1 interfaces which *are* minimizers at some starting $\varepsilon_0 > 0$ we find an $0 < \varepsilon_1 < \varepsilon_0$ such that at ε_1 a branch of minimizing T2 interfaces bifurcates from the T1 branch. Nevertheless, the sequence of tip–interfaces, unstable at sufficently small $\varepsilon > 0$, converges for $\varepsilon \to 0$ to the expected limit (tip) interface and (1.6) holds, i.e., we believe that Remark 1.3(b) also holds in our case of manifolds with conical singularities. We can phrase it as a conjecture.

Conjecture 1.5. *(1.6) also holds for sequences of saddle points of energy, converging to an interface I_0, passing possibly through the conical singularity.*

Additionally, our numerics suggest that for the limit $\varepsilon \to 0$ the main influence of the tip is that for tip–interfaces the convergence in (1.6) is *slower* than for interfaces which avoid the tip. Correspondingly, level-lines such as $u_\varepsilon = \pm\frac{1}{2}$ at small finite $\varepsilon > 0$ keep a larger distance from the interface $u_\varepsilon = 0$ near the tip than in smooth parts of the cones. Moreover, this effect becomes stronger for more pointed cones, i.e., can be seen as a measure of the strength of the singularity.

1.6. **Some related problems.** By Cahn–Hilliard *problem* we denote the elliptic equation (1.4a) together with the mass constraint (1.4b). The dynamic Cahn–

Hilliard *equation* (in Euclidean space) is the mass conserving flow

$$\partial_t u = \nabla \cdot [\nabla \delta_u E_\varepsilon(u)] = -\Delta[\varepsilon^2 \Delta u - W'(u)], \tag{1.7}$$

also called H^{-1} gradient flow, where δ_u denotes the variational derivative. For zero-flux boundary conditions, i.e., $\partial_n u = \partial_n \Delta u = 0$ on $\partial\Omega$, this conserves the mass $\int_\Omega u\,dx$, and steady states of (1.7) fulfill $\varepsilon^2 \Delta u - W'(u) = \lambda$ for some $\lambda \in \mathbb{R}$ and hence are solutions of (1.4).

See [Ell89] for basic results on existence of solutions of (1.7) (in 2D flat domains), their numerical approximation, and their basic dynamical behavior, which can roughly be characterized as follows: Starting from essentially random initial data (with mass 0), the solution rapidly evolves to a fine grained structure with complex interfaces between the phases $u = \pm 1$, also aptly called "fat spaghettis". After this initial phase, a slow coarsening process sets in, during which interfaces move and disappear (regions of pure phases $u \approx 1$ or $u \approx -1$ coming together), on longer and longer time scales. See also [Mir19, DF20] for comprehensive reviews of other Cahn–Hilliard type equations used to describe diffusive interfaces in a variety of settings and applications, and of their analytical and numerical treatment.

The parabolic Allen-Cahn equation is given by

$$\partial_t u - \varepsilon^2 \Delta u + W'(u) = 0,$$

again with Neumann boundary conditions at ∂M. For small ε, the level sets of u concentrate around an interface that evolves in time under a generalized mean curvature flow [ESS92]. However, the mass is in general not conserved. This holds for $\partial_t u - \varepsilon^2 \Delta u + (W'(u) - \langle W'(u) \rangle) = 0$, for which solutions converge to a volume preserving mean curvature flow [CHL10]. It should be interesting to transfer such results to the case of manifolds with conical singularities too. See [RS13, Ver16] for well–posedness results for the Allen–Cahn and Cahn–Hilliard equations on singular manifolds.

1.7. **Structure of the paper.** In §2 we prove Theorem 1.2; in §3 we study length-minimizing area halving–curves on surfaces with conical singularities and prove Proposition 1.4; in §4 we perform numerical bifurcation analysis on cones at finite $\varepsilon > 0$, and then let $\varepsilon \to 0$. In Appendix A we collect some auxiliary analytical results needed for the proof of Thm 1.2, and in Appendix B we collect some basic facts on conical singularities.

Acknowledgments: The authors thank Marco Guaraco for valuable comments.

2. Convergence of minimizers on singular spaces

Throughout, let $\overline{M}$ be a compact manifold with boundary and finitely many conical singularities, and denote by M its regular part, with Riemannian metric g, see Definition B.1.

2.1. **Existence and regularity of solutions.** The results of this subsection in fact hold for general incomplete Riemannian manifolds (M, g) of finite volume. This goes well beyond compact manifolds with boundary and conical singularities. Note that, when we talk about manifolds with boundary here then the letter M denotes the interior, not including the boundary.

However, all the other subsections require the singularities to be conical and the space to be compact.

2.1.1. *Self-adjoint extensions of the Laplacian.* Consider the gradient ∇ on (M, g), mapping smooth functions $C_0^\infty(M)$ to smooth sections of the tangent bundle $C_0^\infty(M, TM)$. We write $\Delta = -\nabla^t\nabla$ for the (negative) Laplace Beltrami operator. If M is a closed compact manifold, then the usual Sobolev spaces

$$\begin{aligned} H^1(M) &:= \{u \in L^2(M) : \nabla u \in L^2(TM)\}, \\ H^2(M) &:= \{u \in H^1(M) : \nabla^2 u \in L^2(\Lambda^2 TM)\}, \end{aligned}$$

define unique closed, and in the latter case unique self-adjoint, extensions of ∇ and Δ, respectively. If (M, g) is non-compact, the extensions may not longer be unique and we shall now employ the formalism of minimal and maximal extensions, as in the seminal work by Brüning-Lesch [BL92].

The maximal and minimal closed (with respect to the graph norm) extensions $\nabla_{\max}, \nabla_{\min}$ are defined by the respective domains

$$\begin{aligned} \mathcal{D}(\nabla_{\max}) &:= \{u \in L^2(M) : \nabla u \in L^2(TM)\} = H^1(M), \\ \mathcal{D}(\nabla_{\min}) &:= \{u \in \mathcal{D}(\nabla_{\max}) : \exists \{u_n\}_n \subset C_0^\infty(M) : \\ &\qquad u_n \xrightarrow{n\to\infty} u, \nabla u_n \xrightarrow{n\to\infty} \nabla u \text{ in } L^2\}. \end{aligned} \tag{2.1}$$

The two extensions define ideal boundary conditions in the sense of Cheeger [Che83] and Brüning-Lesch [BL92] and yield self adjoint extensions of the Laplace Beltrami operator on (M, g)

$$\begin{aligned} \Delta_D &:= -\nabla_{\min}^*\nabla_{\min}, \quad \mathcal{D}(\Delta_D) = \mathcal{D}(\nabla_{\min}^*\nabla_{\min}), \\ \Delta_N &:= -\nabla_{\max}^*\nabla_{\max}, \quad \mathcal{D}(\Delta_N) = \mathcal{D}(\nabla_{\max}^*\nabla_{\max}). \end{aligned} \tag{2.2}$$

The two extensions define the well-known Dirichlet and Neumann boundary conditions in case M is the interior of a compact Riemannian manifold with boundary, $\overline{M} = M \cup \partial M$. We shall be precise: the trace theorem asserts that the obvious restriction, mapping any $u \in C^\infty(\overline{M})$ to $u|_{\partial M} \in C^\infty(\partial M)$ admits a continuous extension

$$\mathrm{tr} : \mathcal{D}(\nabla_{\max}) \to L^2(\partial M), \tag{2.3}$$

where continuity holds with respect to the graph norm on $\mathcal{D}(\nabla_{\max})$ and the L^2 space on the right is defined with respect to the restriction of g to ∂M. Similarly, if ∂_ν is the unit normal inward vector field on ∂M, extended smoothly to the interior, then $u \mapsto \partial_\nu u \restriction \partial M$ admits a continuous extension

$$\operatorname{tr} \circ \partial_\nu : \mathcal{D}(\nabla_{\max}) \to H^{-1/2}(\partial M). \tag{2.4}$$

By continuity of the trace we observe

$$\mathcal{D}(\nabla_{\min}) \subseteq \{u \in \mathcal{D}(\nabla_{\max}) = H^1(M) : \operatorname{tr} u = 0\} =: H^1_0(M). \tag{2.5}$$

The following result is observed in [BL92, §4]. If $\overline{M}$ is non-compact, e.g. it has 'interior singularities', and if $\phi \in C^\infty(\overline{M})$ is compactly supported, i.e. supported *away* from the singularities in the interior, then

$$\begin{aligned} \phi\mathcal{D}(\Delta_D) &= \phi\{u \in H^2(M) : \operatorname{tr} u = 0\}, \\ \phi\mathcal{D}(\Delta_N) &= \phi\{u \in H^2(M) : \operatorname{tr} \circ \partial_\nu u = 0\}. \end{aligned} \tag{2.6}$$

This motivates the choice of the subscripts D and N that stand for Dirichlet and Neumann boundary conditions.

Remark 2.1. See Appendix B for further comments on $\mathcal{D}(\Delta_D)$ and $\mathcal{D}(\Delta_N)$ in the conical case.

2.1.2. *Existence of minimizers.* We begin with the existence of minimizers. For coercive functionals on $\mathbb{R}^d$, this is a classical result, see e.g. [Eva98, Chapter 8]. The proof presented here holds on any finite volume Riemannian manifold, possibly incomplete, including those with conical singularities.

Proposition 2.2. *Consider the function spaces*

$$\begin{aligned} \mathcal{A}_D &:= \{u \in \mathcal{D}(\nabla_{\min}) \cap L^4(M) : \langle u \rangle = m\}, \\ \mathcal{A}_N &:= \{u \in \mathcal{D}(\nabla_{\max}) \cap L^4(M) : \langle u \rangle = m\}. \end{aligned} \tag{2.7}$$

Then for any fixed $\varepsilon > 0$ there exist minimizers $u^\varepsilon_D \in \mathcal{A}_D$ and $u^\varepsilon_N \in \mathcal{A}_N$ such that

$$E_\varepsilon(u^\varepsilon_D) = \inf_{u \in \mathcal{A}_D} E_\varepsilon(u), \quad E_\varepsilon(u^\varepsilon_N) = \inf_{u \in \mathcal{A}_N} E_\varepsilon(u). \tag{2.8}$$

Proof. We prove existence of a minimizer $u_D \equiv u^\varepsilon_D \in \mathcal{A}_D$. The argument for the other case is exactly the same, with $u^\varepsilon_D, \nabla_{\min}, \mathcal{A}_D$ replaced by $u^\varepsilon_N, \nabla_{\max}, \mathcal{A}_N$, respectively. First, consider a sequence $(u_n) \subset \mathcal{A}_D$ such that

$$\inf_{u \in \mathcal{A}_D} E_\varepsilon(u) = \lim_{n \to \infty} E_\varepsilon(u_n).$$

We want to use the Banach-Alaoglu theorem which states that in every reflexive Banach space, every bounded sequence admits a weakly convergent subsequence. First, $\mathcal{D}(\nabla_{\min})$ is indeed a reflexive Banach space: the map $u \mapsto (u, \nabla u)$ identifies $\mathcal{D}(\nabla_{\min})$ with a closed subspace of $L^2(M) \times L^2(M, TM)$; the latter is a reflexive Banach space and thus any closed subspace, such as $\mathcal{D}(\nabla_{\min})$, is a reflexive Banach space as well.

Second, $(u_n) \subset \mathcal{D}(\nabla_{\min})$ is indeed a bounded sequence: $E_\varepsilon(u) \geq 0$ for any $u \in \mathcal{D}(\nabla_{\min}) \cap L^4(M)$ and hence the infimum of $E_\varepsilon(u)$ over $u \in \mathcal{A}_D$ is finite; therefore $(E_\varepsilon(u_n))_n$ has finite limit and in particular is uniformly bounded. This shows boundedness of $(u_n) \subset \mathcal{D}(\nabla_{\min})$ in the graph norm, where we have used that the L^2-norm is bounded by the L^4-norm on manifolds of finite volume.

Thus by the Banach-Alaoglu theorem, there exists a subsequence $(u_{n_k}) \subset \mathcal{D}(\nabla_{\min})$, which is weakly convergent, i.e. there exists $u_* \in \mathcal{D}(\nabla_{\min})$ such that for any $\phi \in L^2(M)$ and $\psi \in L^2(M, TM)$

$$\int_M u_{n_k}\phi \xrightarrow{k\to\infty} \int_M u_*\phi \quad \int_M g(\nabla u_{n_k};\psi) \xrightarrow{k\to\infty} \int_M g(\nabla u_*;\psi). \tag{2.9}$$

Since $(u_{n_k}^2 - 1) \subset L^2(M)$ is a bounded sequence in a reflexive Banach space as well, we can apply Banach-Alaoglu again and assume by passing to a subsequence, that

$$\int_M (u_{n_k}^2 - 1)\phi \xrightarrow{k\to\infty} \int_M (u_*^2 - 1)\phi.$$

Taking the test function $\phi \equiv 1$, we find that weak convergence preserves the mass constraint (1.2), i.e. $\langle u \rangle = m$. Since L^2-norms are weakly lower semicontinuous, we conclude

$$\begin{aligned} \|\nabla u_*\|_{L^2} &\leq \liminf_{k\to\infty} \|\nabla u_{n_k}\|_{L^2}, \\ \|u_*^2 - 1\|_{L^2} &\leq \liminf_{k\to\infty} \|u_{n_k}^2 - 1\|_{L^2}. \end{aligned} \tag{2.10}$$

We conclude that $u_* \in \mathcal{A}_D$ is indeed a minimizer, since by (2.10)

$$E_\varepsilon(u_*) = \frac{\varepsilon}{4\sigma}\|\nabla u_*\|_{L^2} + \frac{1}{4}\|u_*^2 - 1\|_{L^2} \leq \liminf_{k\to\infty} E_\varepsilon(u_{n_k}) = \inf_{u\in\mathcal{A}_D} E_\varepsilon(u).$$

□

The same result holds if we impose additional, e.g. generalized Neumann boundary conditions in the definition of $\mathcal{A}_N$, since the trace operator tr in (2.3) is continuous in the operator norms and in particular weakly continuous. Thus, weak convergence preserves boundary conditions.

The existence in Proposition 2.2 is sufficient to proceed with the convergence of u_ε, and also to justify the numerics in §4. Thus, rather for completeness our next result shows that minimizers are in fact strong solutions of the Allen-Cahn equation. We do not proceed as in Evans [Eva98, §8], but rather present an approach adapted to the present possibly singular setting. Consider the Lagrangian $L(u,\lambda)$ as in (1.3) and note that a minimizer u of $L(u,\lambda)$ satisfies

$$\left.\frac{d}{ds}\right|_{s=0} L(u+s\phi,\lambda) \equiv \varepsilon^2 \int_M g(\nabla u, \nabla\phi) + \int_M W'(u)\phi - \int_M \lambda\phi = 0, \tag{2.11}$$

where we vary among $\phi \in \mathcal{D}(\nabla_{\min})$ if $u \in \mathcal{A}_D$, and $\phi \in \mathcal{D}(\nabla_{\max})$ if $u \in \mathcal{A}_N$. In other words, u in $\mathcal{A}_D$ or $\mathcal{A}_N$ is a weak solution to the Allen-Cahn equation (1.4), with the test functions ϕ lying in $\mathcal{D}(\nabla_{\min})$ or $\mathcal{D}(\nabla_{\max})$, respectively. Note that the intersection with $L^4(M)$ is no longer needed for the test functions.

Proposition 2.3. *Consider any* $u \in H^1(M) \cap L^4(M)$.

1. *Let* u *be a weak solution to the Allen-Cahn equation* (1.4)*, with test functions* $\phi \in \mathcal{D}(\nabla_{\min}) \subseteq H^1_0(M)$. *Then* $u \in \mathcal{D}(\nabla^*_{\min}\nabla_{\min})$ *and in particular,* $\operatorname{tr} u = 0$.
2. *Let* u *be a weak solution to the Allen-Cahn equation* (1.4)*, with test functions* $\phi \in \mathcal{D}(\nabla_{\max}) \equiv H^1(M)$. *Then* $u \in \mathcal{D}(\nabla^*_{\max}\nabla_{\max})$ *and in particular,* $\operatorname{tr} \circ \partial_\nu u = 0$.

Proof. We shall prove the first statement, the second one being verbatim with $\nabla_{\min}$ and Δ_D replaced by $\nabla_{\max}$ and Δ_N, respectively. We may rewrite the Allen-Cahn equation (1.4) as $\Delta u = \varepsilon^{-2}\Big(W'(u) - \lambda\Big)$. Hence u is a weak stationary (i.e. time independent) solution to the inhomogeneous heat equation

$$(\partial_t - \Delta)\, \omega = -\varepsilon^{-2}\Big(W'(u) - \lambda\Big). \tag{2.12}$$

Consider the self-adjoint extension $\Delta_D = -\nabla^*_{\min}\nabla_{\min}$ of the Laplace Beltrami operator on (M, g), with domain $\mathcal{D}(\nabla^*_{\min}\nabla_{\min})$. Consider the heat semigroup $e^{t\Delta_D}$ generated by Δ_D. A solution to (2.12) with initial condition $\omega(0) = u$ is given in terms of the heat semigroup by

$$\omega := e^{t\Delta_D} u - \varepsilon^{-2} e^{t\Delta_D} * \Big(W'(u) - \lambda\Big), \tag{2.13}$$

where $*$ indicates convolution in time. The proof now proceeds by studying regularity of ω and then proving $\omega \equiv u$. Since $u, W'(u) \in L^2(M)$ and the domain of Δ_D is dense in $L^2(M)$, ω is a mild solution to (2.12) in the sense of [Lun95, Definition 4.1.4]. By [Lun95, Theorem 4.3.1], we conclude that ω is in fact a classical solution, i.e. for any $T > 0$ we have the regularity

$$\omega \in C\Big((0, T], \mathcal{D}(\Delta_D)\Big) \cap C^1\Big((0, T], L^2(M)\Big). \tag{2.14}$$

Since $\mathcal{D}(\Delta_D) = \mathcal{D}(\nabla^*_{\min}\nabla_{\min})$, we can integrate by parts for any $\phi \in \mathcal{D}(\nabla_{\min})$

$$\int_M g\big(\Delta_D\, \omega, \phi\big) = -\int_M g\big(\nabla \omega, \nabla \phi\big). \tag{2.15}$$

It remains to show $\omega \equiv u$. By construction, $(\omega - u)$ solves the following equation

$$(\partial_t - \Delta)(\omega - u) = 0, \quad \omega(0) = u,$$

weakly, i.e. for any $\phi \in \mathcal{D}(\nabla_{\min})$ we have (cf. (2.11) and (2.15))

$$\int_M (\partial_t\, \omega)\phi + \int_M g\big(\nabla(\omega - u), \nabla \phi\big) = 0. \tag{2.16}$$

From here we compute by plugging $\phi = (\omega - u)$ into (2.16)

$$\begin{aligned} \frac{d}{dt}\Big\| \omega - u \Big\|_{L^2}^2 &= 2\int_M (\partial_t \omega)(\omega - u) \\ &= -\int_M g\Big(\nabla(\omega - u), \nabla(\omega - u)\Big) = -\Big\|\nabla(\omega - u)\Big\|_{L^2}^2 \leq 0. \end{aligned} \tag{2.17}$$

Thus, if $\|\omega(t) - u\|_{L^2}$ is continuous as $t \to 0$, then (2.17) together with $\omega(0) = u$ implies that $\omega(t) \equiv u$. From here the statement follows with (2.14). Hence it remains to establish continuity of $\|\omega(t) - u\|_{L^2}$ at $t = 0$. Note first

$$\Big\|e^{t\Delta_D} * \Big(W'(u) - \lambda\Big)\Big\|_{L^2} \leq \int_0^t \Big\|e^{(t-\widetilde{t})\Delta_D} * \Big(W'(u) - \lambda\Big)\Big\|_{L^2} d\widetilde{t} \xrightarrow{t \to 0} 0.$$

By the Lumer-Phillips theorem [LP61, Theorem 3.1], the heat operator $e^{t\Delta_D}$ is a strongly continuous semigroup, generated by Δ_D. Indeed, $\Delta_D \leq 0$ is dissipative [LP61, (1.1)] and the image of $(\mathrm{Id} - \Delta_D)$ is $L^2(M)$, since 1 lies in the resolvent set of the closed operator Δ_D. Hence the conditions of the Lumer-Phillips theorem are satisfied and by strong continuity of $e^{t\Delta_D}$

$$\Big\|e^{t\Delta_D} u - u\Big\|_{L^2} \xrightarrow{t \to 0} 0.$$

In view of (2.13), we conclude that $\|\omega(t) - u\|_{L^2} \to 0$ as $t \to 0$ and hence by (2.17) we find $\omega(t) \equiv u$. The statement now follows from (2.14). ☐

2.2. **Convergence.** We want to extend the Modica-Mortola Theorem in [Rin18, Chapter 13.2], stated and proved for domains in $\mathbb{R}^d$, to compact manifolds $\overline{M}$ of dimension d with boundary and conical singularities.

Let $W : \mathbb{R} \to [0, +\infty)$ be a continuous double-well potential with exactly two minima at ± 1, e.g., $W(x) = \frac{1}{4}(x^2 - 1)^2$. Recall from (1.1) that $\sigma = \int_{-1}^1 \sqrt{W(s)/2}\, ds$. Let $|M|_g$ denote the finite volume of (M, g) and fix any mass $m \in (-1, 1)$. The energy functional $E_\varepsilon(u)$ in (1.1) is defined a priori only for $u \in H^1(M) \cap L^4(M)$. We extend its definition to any $u \in L^1(M)$ by a simple trick (recall $\mathcal{A}_N$ is defined in Proposition 2.2)

$$\mathcal{E}_\varepsilon[u] := \begin{cases} E_\varepsilon(u), & \text{if } u \in \mathcal{A}_N, \\ +\infty, & \text{if } u \in L^1(M) \backslash \mathcal{A}_N. \end{cases} \tag{2.18}$$

This extension does not affect the minimizers: indeed the minimizers u_N^ε of $E_\varepsilon(u), u \in \mathcal{A}_N$ are precisely the minimizers of $\mathcal{E}_\varepsilon[u], u \in L^1(M)$.

Consider the space $BV(M; \{-1, 1\})$ of functions $u : M \to \{-1, 1\}$ of bounded variation and recall the notation $\langle u \rangle$ in the mass constraint (1.2). Then we set using the notion of perimeter P_g of Caccioppoli sets in Definition A.8

$$\mathcal{E}_0[u] := \begin{cases} P_g(\{x \in M : u(x) = -1\}) & \text{if } u \in BV(M; \{-1, 1\}), \langle u \rangle = m, \\ +\infty, & \text{otherwise}. \end{cases} \tag{2.19}$$

This measures the size of the boundary of $\{x \in M : u(x) = -1\}$, not including the part of it contained in ∂M. While $BV(M) \subset L^1_{loc}(M)$, restricting the values to $\{\pm 1\}$ gives $BV(M; \{-1, 1\}) \subset L^1(M)$ on manifolds (M, g) of finite volume.

Note also that the minimizers of $\mathcal{E}_0[u], u \in L^1(M)$, are precisely those functions with values ± 1 and satisfying $\langle u \rangle = m$ with a jump along hypersurfaces of minimal perimeter. We begin with a preliminary approximation result, which is where we have to be careful about the conical singularities.

Lemma 2.4. *Consider* $u \in BV(M, \{-1, 1\})$ *with* $\langle u \rangle = m$, *such that* $\mathcal{E}_0[u] < \infty$. *Set* $E = \{x \in M : u(x) = -1\}$. *Then there exists a sequence of subsets* $(E_n)_n \subset M$ *with smooth boundaries* $\partial E_n \subset M \backslash \partial M$ *not intersecting the conical singularities of* M, *such that for* $u_n := -\chi_{E_n} + \chi_{M \backslash E_n}$ *the following holds* ($d = \dim M$)

$$\mathcal{E}_0[u_n] \to \mathcal{E}_0[u], \quad \mathcal{H}^{d-1}(\partial E_n \cap \partial M) = 0, \quad |(E \backslash E_n) \cup (E_n \backslash E)| \to 0. \tag{2.20}$$

Here $|E|$ denotes the volume of the set E.

Proof. Applying [Rin18, Lemma 13.8] locally in each coordinate neighborhood, we can approximate u by $v_n = -\chi_{F_n} + \chi_{M \backslash F_n}$, where (F_n) is a sequence of subsets in M of finite perimeter with boundary that is smooth in the interior of M, and

$$\mathcal{E}_0[v_n] \to \mathcal{E}_0[u], \quad |(E \backslash F_n) \cup (F_n \backslash E)| \to 0.$$

Since each F_n is smooth, and hence F_n and and $M \setminus F_n$ each contain a non-empty open ball, we can apply [Mod87, Lemma 1] or [Rin18, Lemma 13.7] locally in each coordinate chart, to find another approximation by $w_n = -\chi_{G_n} + \chi_{M \backslash G_n}$, where the subsets (G_n) are of finite perimeter, with boundary smooth in the interior of M, and

$$\mathcal{E}_0[w_n] \to \mathcal{E}_0[u], \quad \mathcal{H}^{d-1}(\partial G_n \cap \partial M) = 0, \quad |(E \backslash G_n) \cup (G_n \backslash E)| \to 0.$$

The interfaces ∂G_n may however intersect the conical singularities of M. In order to avoid that, let us assume first that M has a single conical singularity $\mathcal{C}(N) = (0, 1) \times N$. Denote the radial coordinate by $x \in (0, 1)$, and extend it as a smooth function to all of M, with $x \geq 1$ outside $\mathcal{C}(N)$. Sard's theorem applied to the function $x \restriction \partial G_n$ on ∂G_n implies that there exists $\varepsilon_n \in (0, 1/n)$ such that $V_n := \partial G_n \cap \{x = \varepsilon_n\}$ is a smooth submanifold of G_n, for each $n \in \mathbb{N}$. By construction $E'_n := G_n \cap \{x \geq \varepsilon_n\}$ has boundary $\partial E'_n = G'_n \cup G''_n$ where

$$\begin{aligned} G'_n &:= G_n \cap \{x = \varepsilon_n\}, \\ G''_n &:= \partial G_n \cap \{x \geq \varepsilon_n\}, \end{aligned}$$

and the submanifolds G'_n and G''_n intersect each other in their common boundary V_n transversally. The sequence E'_n satisfies (2.20). But $\partial E'_n$ is not smooth at the corner V_n. This setting is illustrated in Figure 2.

However, we may smoothen out the corner as follows. Write $G'_n = \{\varepsilon_n\} \times \tilde{G}'_n$ and $V_n = \{\varepsilon_n\} \times \tilde{V}_n$ with $\tilde{G}'_n, \tilde{V}_n \subset N$. Denote by $y_n : \tilde{G}'_n \to [0, \infty)$ a boundary

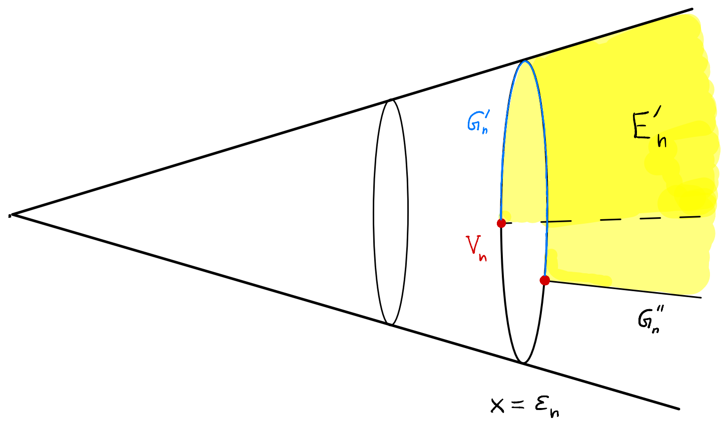

Figure 2: Illustration of V_n, E_n', G_n' and G_n''.

defining function of $\tilde{V}_n$ in $\tilde{G}_n'$, i.e. $\tilde{V}_n = \{y_n = 0\}$ and $\nabla y_n \neq 0$ at $\tilde{V}_n$, and chosen to have 1 in its range as a regular value. Consider a smooth function $\gamma : (\varepsilon_n/2, \varepsilon_n)_x \to (0,1)_{y_n}$ whose graph forms a smooth curve together with the half-lines $(x \geq \varepsilon_n, y = 0)$ and $(x = \varepsilon_n/2, y \geq 1)$. This is illustrated in Figure 3.

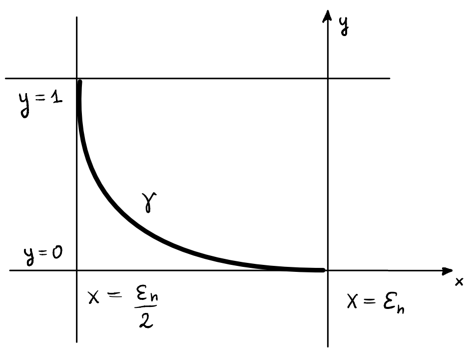

Figure 3: Illustration of curve γ.

We can now smoothen out the corner in E_n' by setting as in Figure 4

$$E_n := E_n' \cup \{(x,q) \in (\varepsilon_n/2, \varepsilon_n) \times \tilde{G}_n' \ : \ \ y_n(q) > \gamma(x)\}.$$

Because E_n differs from G_n only in a small conical neighborhood $(0, \varepsilon_n) \times N$ with $\varepsilon_n \to 0$ as $n \to \infty$, (E_n) satisfies (2.20), and this proves the statement. In the general case of finitely many conical singularities, we repeat such procedure in each conical neighborhood. □

We can now prove our main result here, namely the Γ-convergence of the functionals above.

Theorem 2.5. *$\mathcal{E}_\varepsilon$ Γ-converges to $\mathcal{E}_0$ as $\varepsilon \to 0^+$ with respect to the strong L^1-topology.*

Proof. To prove Γ-convergence we need to prove the lim inf-inequality (A.3) and additionally, by Remark A.10, construct a sequence that fulfills the lim sup-inequality (A.5). The underlying complete metric space is $L^1(M)$.

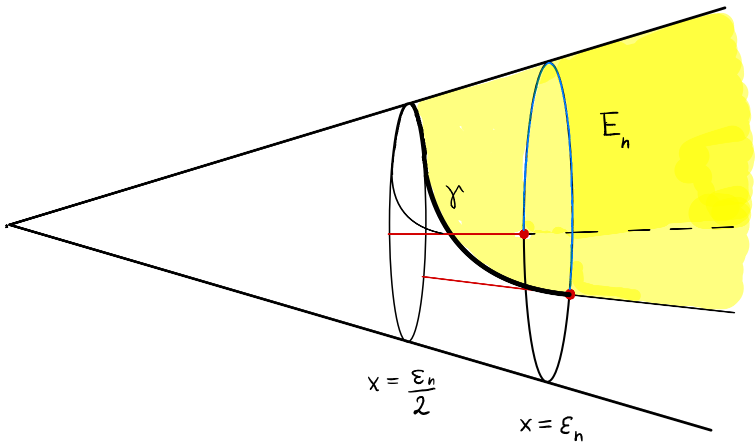

Figure 4: Illustration of E_n.

We shall start with the lim inf-inequality. Let $u_\varepsilon \longrightarrow u$ in $L^1(M)$ as $\varepsilon \to 0$ and assume $\liminf_{\varepsilon \to 0} \mathcal{E}_\varepsilon[u_\varepsilon] < \infty$ (otherwise there is nothing to prove), i.e. we may assume without loss of generality that $u_\varepsilon \in \mathcal{A}_N$ for all $\varepsilon > 0$. Consider a subsequence $\varepsilon_n \longrightarrow 0$ such that $u_{\varepsilon_n} \to u$ pointwise almost everywhere as $n \to \infty$. Then by Fatou's lemma we obtain

$$
\begin{aligned}
0 \leq \int_M W(u) &= \int_M \liminf_{n\to\infty} W(u_{\varepsilon_n}) \leq \liminf_{n\to\infty} \int_M W(u_{\varepsilon_n}) \\
&\leq \liminf_{n\to\infty} \int_M \frac{\varepsilon_n^2}{2} |\nabla_g u_{\varepsilon_n}|^2 + W(u_{\varepsilon_n}) = \liminf_{n\to\infty} 2\sigma\varepsilon_n \mathcal{E}_{\varepsilon_n}[u_{\varepsilon_n}] = 0,
\end{aligned}
$$

because $\liminf_{n\to\infty} \mathcal{E}_{\varepsilon_n}[u_{\varepsilon_n}] < \infty$. Hence, $W(u) = 0$ and thus also u takes values in $\{-1, 1\}$ almost everywhere. Furthermore, we compute

$$
\begin{aligned}
\liminf_{n\to\infty} \mathcal{E}_{\varepsilon_n}[u_{\varepsilon_n}] &= \liminf_{n\to\infty} \frac{1}{2\sigma} \int_M \frac{\varepsilon_n}{2} |\nabla_g u_{\varepsilon_n}|^2 + \frac{1}{\varepsilon_n} W(u_{\varepsilon_n}) \\
&\geq \liminf_{n\to\infty} \int_M \frac{1}{\sqrt{2}\sigma} |\nabla_g u_{\varepsilon_n}| \sqrt{W(u_{\varepsilon_n})} \geq \liminf_{n\to\infty} \int_M \frac{1}{\sqrt{2}\sigma} |\nabla_g (h \circ u_{\varepsilon_n})| \\
&\geq \frac{1}{\sqrt{2}\sigma} \|\nabla_g (h \circ u)\|_g(M) = \frac{(h(1) - h(-1))}{\sqrt{2}\sigma} P_g(\{x \in M : u(x) = -1\}) \\
&= P_g(\{x \in M : u(x) = -1\}) \equiv \mathcal{E}_0[u],
\end{aligned}
$$

where $h(t) := \int_0^t \sqrt{W(s)}\,ds$ and we used (A.1) in the last inequality step. This proves the lim inf-inequality.

In the second step we have to construct a recovery sequence $(u_\varepsilon)_\varepsilon$ that converges to u in $L^1(M)$ and fulfills the lim sup-inequality (A.5). If $\mathcal{E}_0[u] = \infty$, there is nothing to prove and hence we assume without loss of generality that $\mathcal{E}_0[u] < \infty$ and thus $u \in BV(M, \{-1, 1\})$ and $\langle u \rangle = m$.

Note that we do not assume that u is a minimizer of $\mathcal{E}_0$, hence the interface ∂E need not be smooth, even for a compact smooth M. In view of Lemma 2.4 however, we may assume without loss of generality that in our quest for a recovery sequence, $u \in BV(M, \{-1, 1\})$ has the property that E is of finite perimeter, has smooth boundary disjoint from conical singularities and satisfies $\mathcal{H}^{d-1}(\partial E \cap \partial M) = 0$. Also, we may assume that E is open. Since ∂E may be assumed to be disjoint from the conical singularities, the remainder of the argument is performed as in the non-singular case.

The construction of the recovery sequence $(u_\varepsilon)_\varepsilon$ is nowadays classical, see [Mod87, Prop. 2 p. 133] and also [Rin18, Theorem 13.6, p. 383-386] for open subsets of $\mathbb{R}^n$. Instead of repeating the steps therein, we refer to the Riemannian version e.g. in [BNAP22, Proposition 3.3], which constructs $(u_\varepsilon)_\varepsilon$ such that

$$\limsup_{\varepsilon \to 0^+} \mathcal{E}_\varepsilon[u_\varepsilon] \le P_g(E, M) \equiv \mathcal{E}_0[u].$$

The construction is local near the smooth boundary ∂E. Since by assumption ∂E is disjoint from the conical singularity, the arguments remain unchanged in our setting. By Remark A.10 Γ-convergence now follows. □

A fundamental consequence of Γ-convergence is convergence of minimizers and the abstract result [Mod87, Proposition 4] together with Theorem 2.5 implies the following

Proposition 2.6. *For every $\varepsilon > 0$, let $u_\varepsilon \in L^1(M)$ be a minimizer of $\mathcal{E}_\varepsilon$. If $u_\varepsilon \to u$ in $L^1(M)$ as $\varepsilon \to 0^+$, then u is a minimizer of $\mathcal{E}_0$ in $L^1(M)$ and $\lim_{\varepsilon \to 0^+} \mathcal{E}_\varepsilon(u_\varepsilon) = \mathcal{E}_0(u)$.*

3. Minimizers on cones in 2D: interfaces

To study the limits at $\varepsilon = 0$ of minimizers of (1.4) in a singular setting, we use truncated cones of height h with elliptic base at $z = 0$ of semi axes 1 and $a \ge 1$, parameterized over the unit disk, i.e.

$$\begin{pmatrix} \tilde{x} \\ \tilde{y} \\ \tilde{z} \end{pmatrix} = \phi(x, y) := \begin{pmatrix} ax \\ y \\ h(1 - (x^2 + y^2)^{1/2}) \end{pmatrix}, \quad (x, y) \in \Omega = \{x^2 + y^2 \le 1\}. \tag{3.1}$$

In view of the forthcoming results in §4.2–§4.6, we first discuss the three types of limit interfaces which we expect from the types T1 (tip), T2 (winding), and T3 (horizontal) from Fig.1 for $\varepsilon \to 0$. They divide the area into two equal halves since $m = 0$, and by the general theory they are critical points of the length functional, so they have constant curvature (except possibly where they pass through the conical singularity), and we call their respective lengths l_1, l_2 and l_3.

We have two results on the question which interface type is a length minimizer. The first is semi–analytical, giving a rather explicit computation of the interface lengths at $\varepsilon = 0$ on a circular cone. See also Fig. 12(b_1) for a comparison with E_ε for the respective solutions at small $\varepsilon > 0$.

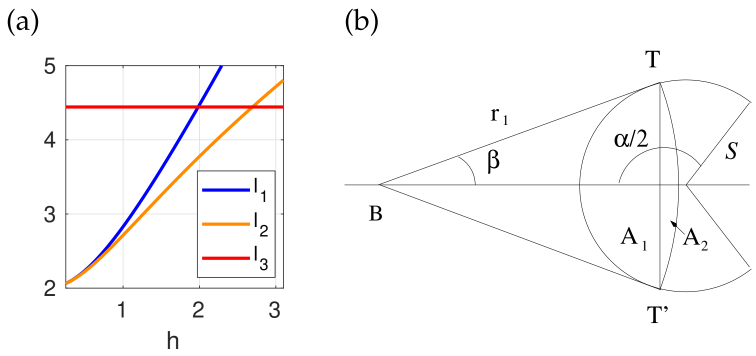

Figure 5: (a) $l_j(h)$. (b) Sketch for computing l_2. The pacman shape arises from cutting open the cone along a radius, and flattening it into the plane.

Result 3.1. *On a circular cone ($a = 1$ in (3.1)) the lengths l_j behave as in Figure 5(a) as a function of the height h of the cone. In particular, the tip interface is never a minimizer, and the circular interface is a minimizer for large h.*

Proof. The slant height of the circular cone of height h is $S = \sqrt{1+h^2}$, so

$$l_1(h) = 2\sqrt{1+h^2}\,.$$

The cone can be explicitly flattened to a circular sector C of radius S and angle $\alpha = 2\pi/\sqrt{1+h^2}$, see Fig. 5(b), and hence area $A = \alpha S^2/2 = 2\pi\sqrt{1+h^2}$. Then,

$$l_3 = \sqrt{2}\pi : \text{ circular interface at height } \tilde{h} = (1 - 1/\sqrt{2})h.$$

Finally, $l_2(h)$ can be computed semi–analytically as follows: First we seek the point T such that the circular arc from T to its reflection T' divides C into two equal areas $\alpha S^2/4$. For given T, the intersection of the tangent to the circle at T with the x–axis is at $x_B = -S/\sin(\beta)$ relative to the center, and the areas $A_1(\beta)$ and $A_2(\beta)$ of the two circular segments to the right and left of the line $\overline{TT'}$ are given by

$$A_1(\beta) = \frac{r_1^2}{2}(2\beta - \sin(2\beta)), \text{ and } A_2(\beta) = \frac{S^2}{2}(\pi - 2\beta - \sin(2\beta)), \tag{3.2}$$

where $r_1 = S\cot\beta$. Thus, we first numerically solve $A_1(\beta) + A_2(\beta) = \alpha S^2/4$ for $\beta \in (0, \pi/2)$, and then compute the length $l_2(h) = 2\beta r_1$. □

The next result applies to surfaces with general conical singularities of angle $\alpha < 2\pi$, which for instance applies to the conic metric $dr^2 + c^2r^2d\theta^2$ on $(0,1) \times S^1$ with angle $\alpha = 2\pi c$ if and only if $c < 1$, and to the elliptic cones (3.1) with general $a \geq 1$, where $\alpha < 2\pi$ if $h > 0$, while naturally $\alpha = 2\pi$ if $h = 0$. Conical surfaces with angles bigger than 2π can be constructed as follows, see also Appendix B for further discussion. If we choose a simple closed curve in the unit sphere in $\mathbb{R}^3$ and take M to be the union of segments $0p$ for p on the curve then we obtain a conical surface with the angle α being the curve length. If $\alpha \geq 2\pi$, then minimizers may in general pass through the singularity (as is the case for a flat disk, which has $\alpha = 2\pi$, where any diameter is a minimizer for $m = 0$), but we now show that tip interfaces are never minimizers for $\alpha < 2\pi$.

Proposition 3.2. *Let $\overline{M}$ be a surface with a conical singularity P of angle $\alpha < 2\pi$. Then any curve of minimal length which divides $\overline{M}$ into two parts of prescribed area ratio does not pass through P.*

Prescribing an area ratio corresponds to choosing a general mass parameter m with $|m| < 1$ in (1.4)(b). The case $m = 0$ corresponds to equal areas. (For elliptic cones it was natural to consider only $m = 0$ because of reflection symmetry.)

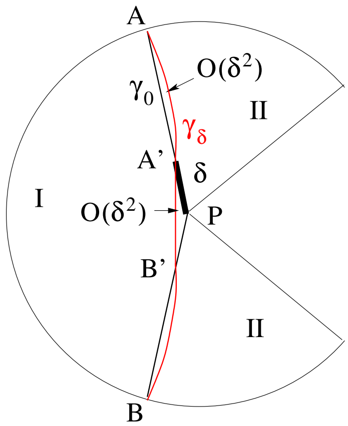

Figure 6: Modifying a tip interface γ_0 to a shorter interface γ_δ.

Proof. Let γ_0 be a curve of minimal length satisfying the area constraint, and assume that it passes through the tip P. We refer to Fig. 6 for a sketch (compare Fig. 5(b)), and construct a shorter such curve γ_δ. Consider a neighborhood U of P in M of the form $(0, 1) \times S^1$ (see Appendix B), on which γ_0 consists of a part AP entering P and a part PB leaving P. Each part has constant curvature, since γ_0 is assumed to be of minimal length. In Fig. 6 they are depicted as straight lines for simplicity.

Denote the components of $U \setminus \gamma_0$ by I and II; because the angle at P is less than 2π at least one of them, say I, has an angle less than π at P. For small $\delta > 0$ let A', B' be points on PA, PB at distance δ from P.

The main point is this: Replacing the part $A'PB'$ of γ_0 by the straight geodesic segment $A'B'$ reduces its length linearly, i.e. by $\geq c\delta$ where $c > 0$. On the other hand, the area of the triangle $A'PB'$ is only $O(\delta^2)$ since a δ-neighborhood of P has area $O(\delta^2)$, so the area of I and II is changed only by $O(\delta^2)$.

Therefore, we can replace the segments AA' and BB' by curves from A to A', and from B to B', respectively, which bulge into II by $O(\delta^2)$, so that the curve γ_δ obtained from this still satisfies the area constraint and has length $\ell(\gamma_0) - c\delta + O(\delta^2)$, which is less than $\ell(\gamma_0)$ for small $\delta > 0$. □

4. Minimizers on cones: Numerical illustrations

4.1. The setup, and basic notions from bifurcation theory. To illustrate Theorem 1.2 and study the minimizers of (1.4) for small $\varepsilon > 0$ in a singular setting we use the truncated cones of height h and semi axes 1 and $a \geq 1$ as in (3.1). The metric determinant is $g = a^2 + h^2(x^2 + ay^2)/r^2$, and $dS = \sqrt{g}\, d(x, y)$, and the corresponding Laplace Beltrami operator is given by

$$\begin{aligned} \Delta u(x, y) = \frac{1}{\sqrt{g}} \Big[& \partial_x \big(\frac{1}{\sqrt{g}}(1 + h^2 y^2 r^{-2})\partial_x u\big) - \partial_y \big(\frac{1}{\sqrt{g}} h^2 xyr^{-2}\partial_x u\big) \\ & - \partial_x \big(\frac{1}{\sqrt{g}} h^2 xyr^{-2}\partial_y u\big) + \partial_y \big(\frac{1}{\sqrt{g}}(a^2 + h^2 x^2 r^{-2})\partial_y u\big) \Big], \end{aligned} \tag{4.1}$$

where the coefficients in the divergence form are L^∞, but not C^0. We choose the standard double well potential $W = \frac{1}{4}(u^2 - 1)^2$, and the energy

$$E_\varepsilon = \frac{1}{2\sigma} \int_\Omega \frac{\varepsilon}{2} |\nabla u|^2 + \frac{1}{\varepsilon} W(u)\, dS,$$

where $\sigma = \int_{-1}^1 \sqrt{W/2}\, du = \sqrt{2}/3$. To recall, our problem thus is

$$\begin{aligned} &\text{(a)} \quad G(u) := -\varepsilon^2 \Delta u + W'(u) - \lambda \stackrel{!}{=} 0 \text{ in } \Omega, \quad \partial_\nu u = 0 \text{ at } \partial\Omega, \\ &\text{(b)} \quad q(u) := \langle u \rangle - m \stackrel{!}{=} 0. \end{aligned} \tag{4.2}$$

We use the software pde2path [Uec21, Uec23b] to discretize (4.2) by the Finite Element Method (FEM), and to treat the obtained algebraic system as a continuation and bifurcation problem. More specifically, we consider the weak form of (4.2a) and hence find critical points of E_ε in $H^1(M)$. For all m, (4.2) has the spatially homogeneous solution $u \equiv m$, $\lambda = W'(m)$, i.e., we have the "trivial branch" $u \equiv m$, with $E_\varepsilon(u) = \frac{1}{2\sigma\varepsilon} W(m)$. Starting at $m = 1$ we first find branch points (BPs) from this trivial branch, and continue the bifurcating branches to $m = 0$ at fixed $h, \varepsilon > 0$ and $a \geq 1$, thus obtaining a selection of critical points u of E_ε at $m = 0$. Subsequently we continue some of these solutions $u_{\varepsilon,h,a}$ in other parameters, including $\varepsilon \to 0$, aiming to identify limits u_0 and the associated interfaces I_0, to check the formula $|I_0| = \lim_{\varepsilon \to 0} E_\varepsilon(u_{\varepsilon,h,a})$, and to altogether identify minimal interfaces (depending on h and a).

By varying a and h we study the dependence of minimizers on the cone geometry; additionally, choosing $a \neq 1$ is useful to break symmetry: For $a = 1$ we have a circular base, and altogether an $O(2)$ equivariant problem, which inter alia means that

- all bifurcations from the spatially homogeneous branch with angular dependence are double, i.e. the linearization at the branch point has a two-dimensional kernel;
- to continue such branches we need a phase condition to uniquely choose solutions from the group orbit of rotations.

pde2path has methods to deal with these issues, but the situation is somewhat simpler and more generic if the rotational symmetry is broken. For elliptic cones, the BPs from the trivial branch are generically simple and hence we can apply the Crandall–Rabinowitz Theorem [CR71] to obtain the bifurcating branches, while for circular cones we would need equivariant bifurcation theory ([Uec21, §2.5] and the references therein), and also the numerics would become slightly more involved. However, we still have three discrete symmetries:

$$\gamma_1: \quad (u(x,y), m, \lambda) \mapsto (u(-x,y), m, \lambda), \quad \mathbb{Z}_2 \text{ symmetry over the } y \text{ axis}; \tag{4.3}$$

$$\gamma_2: \quad (u(x,y), m, \lambda) \mapsto (u(x,-y), m, \lambda), \quad \mathbb{Z}_2 \text{ symmetry over the } x \text{ axis}; \tag{4.4}$$

$$\gamma_3: \quad (u(\cdot,\cdot), m, \lambda) \mapsto (-u(\cdot,\cdot), -m, -\lambda), \quad \begin{array}{l}\mathbb{Z}_2 \text{ symmetry in } u, \text{ mass} \\ \text{and Lagrange multiplier.}\end{array} \tag{4.5}$$

These symmetries generate the symmetry group Γ of the problem via composition. γ_3 can essentially be exploited to restrict to $m \le 0$, and the two mirror symmetries γ_1, γ_2 can be used to *a priori* determine whether bifurcations from simple BPs on the trivial branch are *transcritical* or *pitchforks*, see Remark 4.2.

Remark 4.1. For convenience, here we recall the basic examples (normal forms) for steady bifurcations, referring to [Uec21] and the references therein for further terminology and details, in particular [Kuz04]. Consider the following scalar bifurcation problems, with $\mu \in \mathbb{R}$ as a (generic) parameter.

(a) $f(u,\mu) = \mu - u^2 = 0$. This has the *solution branch* $u = \pm\sqrt{\mu}$ for $\mu \ge 0$, which shows a *fold* at $\mu = 0$. This is also called *saddle-node* bifurcation as the lower branch $u = -\sqrt{\mu}$ contains saddles (unstable solutions) for the ODE $\dot{u} = f(u,\mu)$, while the upper branch contains stable nodes, see Fig. 7(a), which also shows the associated energy $E = -\mu + \frac{1}{3}u^3$ such that $\dot{u} = -E'(u)$. [3]

(b) $f(u,\mu) = \mu u + u^2$. For all $\mu \in \mathbb{R}$ we have the trivial solution $u = 0$, and additionally the "non–trivial branch" $u = -\mu$. $u = 0$ is stable (unstable) for $\mu < 0$ ($\mu > 0$), while $u = -\mu$ is stable (unstable) for $\mu > 0$ ($\mu < 0$). Thus, at the *branching point* $(u,\mu) = (0,0)$ there is an *exchange of stability*. The bifurcating branch $u = -\mu$ exists on both sides of the critical value $\mu = 0$ and hence the bifurcation is called *transcritical*, see Fig. 7(b).

(c) $f(u,\mu) = \mu u - u^3$. As in (b), the trivial solution $u = 0$ is locally unique, except at $\mu = 0$, where the non–trivial branches $u = \pm\sqrt{\mu}$, $\mu > 0$ bifurcate. Moreover, $u = 0$ is stable (unstable) for $\mu < 0$ ($\mu > 0$), and $u = \pm\sqrt{\mu}$ are both stable. This is called a *supercritical pitchfork*, see Fig. 7(c), while for instance for $f(u,\mu) = \mu u + u^3$ we obtain a *subcritical* pitchfork with the bifurcating unstable branches $u = \pm\sqrt{-\mu}$.

(a),(b) and (c) (and further types of bifurcations) can occur along a single branch; for instance, $f(u,\mu)=\mu u+u^3-u^5$ yields a subcritical pitchfork at $(u,\mu) = (0,0)$, with the nontrivial branches stabilizing in folds at $(u,\mu) = (\frac{\pm 1}{\sqrt{2}}, \frac{-1}{4})$. The scalar normal forms typically arise as *bifurcation equations* via Liapunov–Schmidt reduction of, e.g., a PDE problem where along a solution branch a simple eigenvalue of the linearization goes through 0 (bifurcation from simple eigenvalues), where a non-trivial kernel of the linearization is a necessary con-

[3] Any scalar ODE is a gradient system $\dot{u} = -E'(u)$, and if E is bounded below and has only isolated critical points, then any solution must converge to a critical point of E.

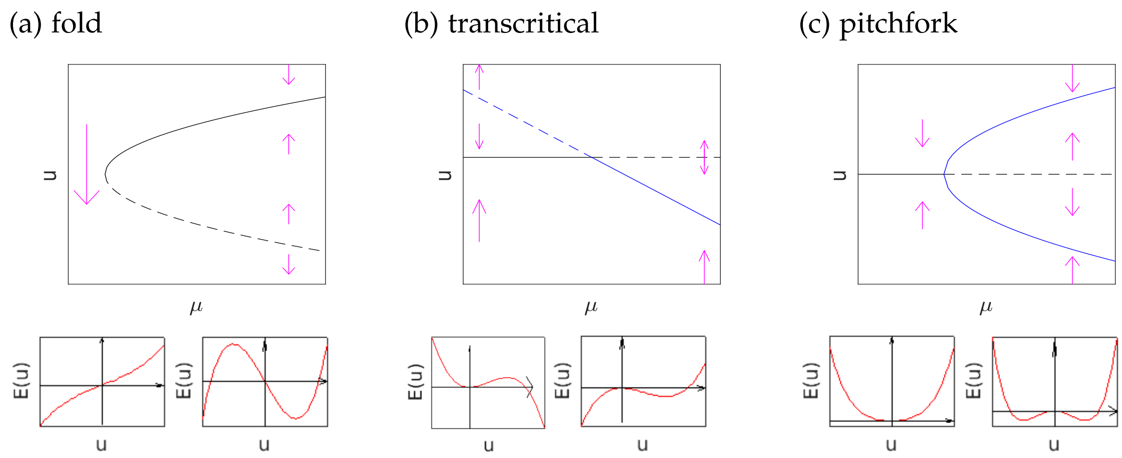

Figure 7: (a-c) Elementary steady bifurcations. Full lines indicate branches of stable solutions and dashed lines indicate unstable branches, with the arrows indicating the flow of the associated ODE $\dot{u} = f(u, \mu) = -\partial_u E(u, \mu)$, with the energies indicated below the bifurcation diagrams at the respective left and right ends in μ for each of the cases.

dition for (steady) bifurcation due to the implicit function theorem. Importantly, only the saddle–node bifurcation (a) is *generic*, while (b) and (c) require some special structure to occur generically, for instance the $\mathbb{Z}_2$ symmetry $u \mapsto -u$ in case of (c). Such symmetries often arise from physics, or in case of PDEs from the considered domain, again see [Uec21, §2.5] for further discussion, and [GS02, Hoy06]. Finally, note that we obtain the smooth plots in (a)–(c) because we consider 1D systems; in higher dimensions, for instance the "shape of folds" strongly depends on the chosen projection (the chosen functional on the ordinate) for plotting the BDs. See for instance Fig.9(a_1) vs Fig.9(d). ⌋

Remark 4.2. In terms of the notions recalled in Remark 4.1, the symmetries γ_1 and γ_2 have the following consequences for bifurcations of nontrivial branches from the trivial branch $u \equiv m$ in (4.2):

- If the solutions u on the bifurcating branch satisfy exactly one of the conditions $\gamma_1 u = u$, $\gamma_2 u = u$ then the bifurcation must be a pitchfork, as together with u also its partner $\gamma_j u$ must bifurcate, $j = 1, 2$. This for instance applies to the branches yielding the tip (T1) and winding (T2) interfaces from Fig. 1.
- Solutions which violate both symmetries γ_1 and γ_2 cannot bifurcate from the homogeneous branch in a simple BP, i.e., they must arise in secondary bifurcations. (We do not further consider such solutions here).
- On the other hand, branches with solutions satisfying both symmetries $\gamma_1 u = u = \gamma_2 u$ (e.g., "horizontal" solutions like in Fig. 1(c), T3) generically bifurcate transcritically from the homogeneous branch. ⌋

Remark 4.3. Besides the 1–parameter bifurcation problems from Remark 4.1, in practice one often has to deal with $n \geq 2$–parameter problems, e.g., the 4–parameter (m, ε, h, a) problem (4.2). In these, often one can fix $n-1$ parameters and let just one parameter vary, but there may be *co–dimension* ℓ points in parameter space, where one needs $\ell \geq 2$ parameters to capture the behavior of the system. One of the simplest examples is the so called *cusp catastrophe* [Kuz04, §8.2], with normal form $f(u, \mu_1, \mu_2) = -4u^3 + 2\mu_1 u - \mu_2$, see Fig.8. For $\mu_1 \le 0$ we always have exactly one stable solution of $f(u, \mu_1, \mu_2) = 0$ for all μ_2, but for $\mu_1 > 0$ we have three solutions between the two fold–curves $\mu_2 = \pm\mu_2(\mu_1)$, with the middle solution unstable and the two other solutions stable, and where the two fold curves form a cusp at the co–dimension two point $(\mu_1, \mu_2) = (0, 0)$. To compute such cusps, it is often useful to compute the fold–curves by *fold point continuation* [Uec21, §3.6.1], [Uec23a]. See Fig. 10 for an example for (4.2). ⌋

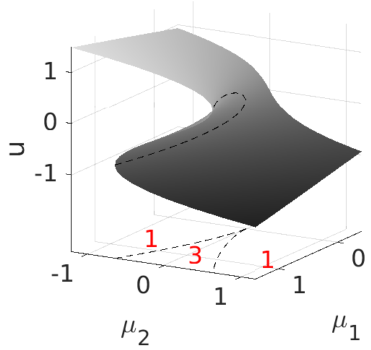

Figure 8: The solution surface of $f(u, \mu_1, \mu_2) := -4u^3+2\mu_1 u-\mu_2 = 0$, and the projection $\mu_2 = \pm\mu_2(\mu_1)$ of the fold curves on the μ_1–μ_2 plane, forming a cusp.

4.2. **Organization of the continuation in the different parameters.** Given the remarks from §4.1 and the results from §3, we organize the numerical continuation at $\varepsilon > 0$ as follows.

- In Fig.9 we compute the basic branches (in m) at fixed $(h, \varepsilon) = (1, 0.15)$ and $a = 1.05$; the latter yields a small deviation from the circular cone to break the rotational invariance.
- In Fig.10 we continue folds which occur in Fig. 9 in h, which shows that the relation of T1 and T2 solutions is similar to the cusp in Remark 4.3.
- In Fig.11 we continue solutions at $m = 0$ from Fig. 9 to smaller ε, essentially verifying the main analytical result that $u_\varepsilon \to u_0$ for a limit function u_0, and $E_\varepsilon(u_\varepsilon) \to |I_0|$, as $\varepsilon \to 0$.
- In Fig. 12 we fix $\varepsilon = 0.1$ and $m = 0$, and study the dependence of T1, T2 and T3 solutions (and their energies) on h and a.

One main result is that at small $\varepsilon > 0$ we generally get results similar to Fig. 5(a), see for instance Fig. 12(b), but also important differences: At small $\varepsilon > 0$, a tip interface is a minimizer for sufficiently large a (depending on h), and the winding T2 interface does not exist (is not a critical point), Fig. 12(e,f), but for $\varepsilon \to 0$ the T2 interface "appears" (bifurcates from the T1 branch) and becomes the minimizer.

4.3. **The basic branches at** $(h, a, \varepsilon) = (1, 1.05, 0.15)$**.** In Fig. 9 we run "continuation in m" at fixed $(h, a, \varepsilon) = (1, 1.05, 0.15)$. This means that m (additional to the Lagrange multiplier λ for the mass constraint $\langle u\rangle = m$) is the free parameter, which may move back and forth, as all continuation is done in so–called arclength parametrization [Uec21].

The black branch hom in the bifurcation diagram (BD) in (a_1) represents the homogeneous solutions $u \equiv m$ with $\lambda{=}W'(m)$ and $E(u){=}\frac{1}{2\sigma\varepsilon}W(m)$. On hom we find (at this relatively large ε) 14 BPs up to $m{=}0$, and we follow the branches bifurcating

- at BP1 (b1, blue, containing type T1 *and* T2 at $m = 0$, see below for further discussion),
- at BP2 (b2, green, like b1 but rotated by 90°),
- at BP3 (b3, red, containing type T3 at $m = 0$),
- and at BP5 (b5, magenta); this is for illustration of just one "higher order branch".

In the following we shall focus on branches b1 and b3. In the BDs, thick lines indicate stable parts of branches (local minima), and thin lines indicate unstable parts (saddles). The BD in (a_1) and those following are essentially verbatim outputs of pde2path scripts, with some postprocessing to adjust labels, subsequently used as identifiers in solution plots. We start the labeling with A at $m = 0$ in panel (a_2) as $m = 0$ will be our interest in the following pictures, while labels I–K are for further illustration only. Open circles indicate detected BPs. In (a_2) we zoom in on the branches b1, b2 near $m = 0$, and in (a_3) on b3 near $m = 0$. In (b,c) we give sample solutions as labeled in (a), and in (d) we present (a_1) for $m \in (-0.8, -0.45)$ in another projection, namely $\max(u) - m$.[4] The b1 solutions fulfill γ_2 (reflection in y), but not γ_1, and hence b1 must bifurcate in a pitchfork. The bifurcation is subcritical but the branch stabilizes in a first fold near $m = -0.79$. On the other hand, solutions on b3 fulfill γ_1 and γ_2 and bifurcate transcritical, as expected. Here, the subcritical part (to more negative m) also folds back and stabilizes.

The first sample plot A in (b) shows the solution on the cone, and also gives the energy E_ε in the title. The second sample in (b) shows the contour lines $u = 0.5$ (red) and $u = -0.5$ (blue) for the same solution A, with the base of the cone indicated in black, and subsequently we mostly use this plot–style. The sample B shows u at the fold point at $m \approx 0.03$, which will be further discussed in Fig. 10. Together, A–C show that b1 approaches $m = 0$ from the left as type T2 solution, and after the fold turns into a T1 solution C with a slightly larger energy. Subsequently, b1 continues symmetrically through the left fold and again past $m = 0$ to the symmetric BPs on hom at $m > 0$. Essentially the same happens on b2, but rotated by 90° such that the T1 interface in E is along the $a = 1.05$ semiaxis, with hence a (slightly) larger energy E than in C. Thus, for b1 and b2 the T1 solution is related to the T2 solutions via folds, similar to the "middle surface" between the two fold–curves in Fig.8, and in Fig.10 we shall illustrate the cusp underlying this.

[4] While this more clearly shows the structure of solutions near bifurcation, in the following we restrict to plotting E_ε, as this is the quantity of interest.

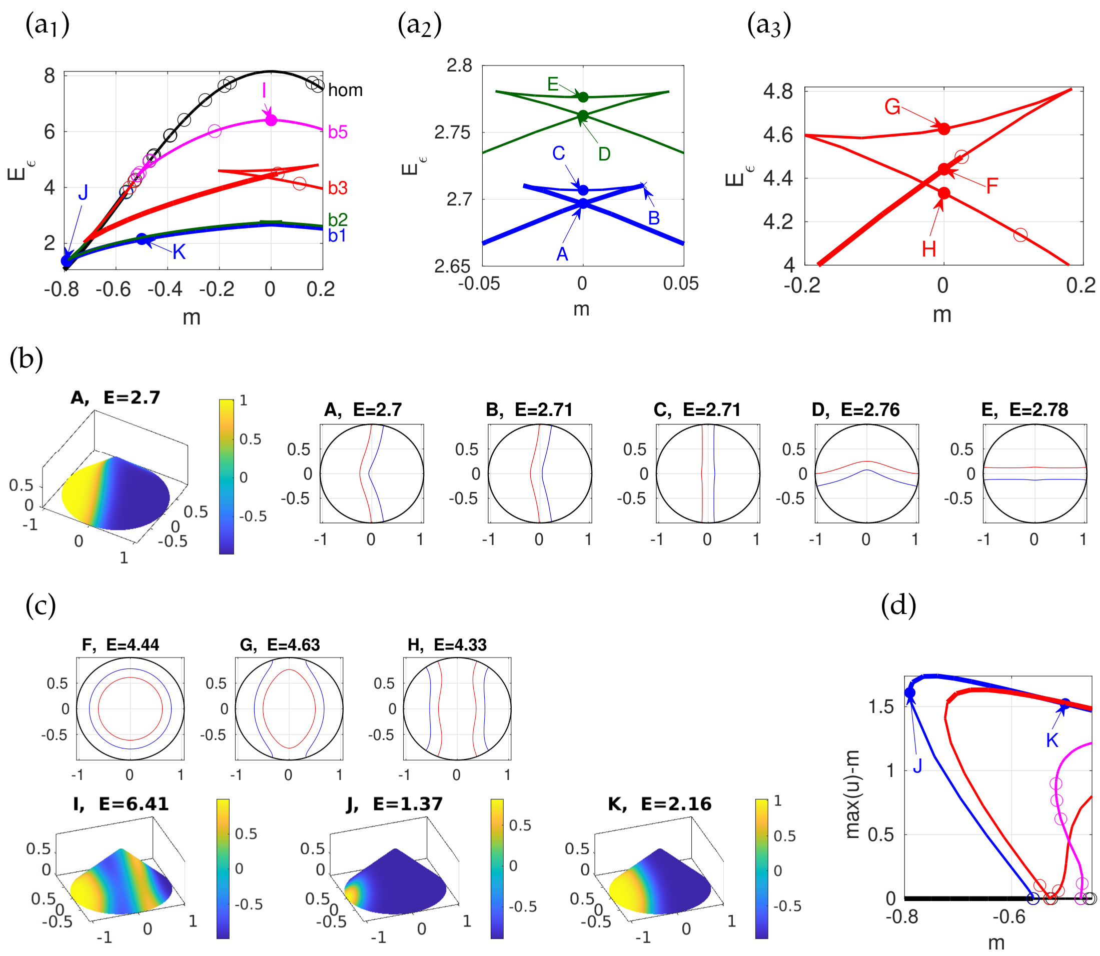

Figure 9: (a) BD for continuation in m, for $(h, a, \varepsilon) = (1, 1.05, 0.15)$, with two zooms near m=0. Primary branches bifurcating from $u \equiv m$ (black branch hom in (a_1)): b1 (blue), b2 (green), b3 (red), and b5 (magenta). (b,c) Sample solutions from (a), as indicated by labels. (d) same as (a_1), plotting $\max(u) - m$ over m (near $m = -0.6$) for b1, b3, and b5.

The samples F–H in (c) show three passages of b3 through $m = 0$. As already said, the bifurcation of b3 is transcritical as the solutions on it fulfill both, γ_1 (reflection in x) and γ_2 (reflection in y), but in (a_1) and (a_3) we only show the subcritical part; this returns supercritically to the symmetric BP at $m > 0$. The most relevant sample on b3 at $m = 0$ is the T3 solution F, as it has the lowest energy among F–H, and is in fact locally stable.

Sample I in (c) belongs to b5. This is only meant as just one example of the many further solutions of (4.2), containing more interfaces than the basic types T1, T2 and T3, and hence not expected to be energy minimizers also when varying other parameters. In particular, for $\varepsilon \to 0$ such solutions may turn into so called $2n$–end types [KLPW15], $n > 1$, i.e., they may contain points where $2n \geq 4$ different phase domains $u = \pm 1$ meet. Specifically, sample I contains two four–end points for $\varepsilon \to 0$, see I in Fig.11(b) for illustration. Finally, samples J (at the first fold of b1) and K in panel (c) are meant to illustrate how b1 proceeds from negative m to $m = 0$ first reached at A; solutions on the other branches behave correspondingly.

4.4. **Fold–continuation in h.** In Fig.10 we show the continuation of the fold at $m = m_0 \approx 0.03$ on b1 (sample B in Fig.9). In brief, this illustrates the cusp structure of the relation between T1 and T2 solutions. In detail, on the part containing B in Fig.10, the fold location increases with h, see sample B^+, which also implies that the T1 and T2 solutions separate more strongly with increasing h. Conversely, decreasing h from $h = 1$ the fold position goes to $m = 0$, where it continues as the symmetric fold to sample B^-. In particular, the collision of the two folds at the cusp $(m, h) = (0, h_c)$, $h_c \approx 0.8$, means that for $h < h_c$ we only have one solution of type T1 or T2, and by symmetry this must be of type T1 (straight interface). This is an important difference to Fig.5(b), where at $\varepsilon = 0$ the type T2 interface exists for all $h > 0$ and coincides with T1 only in the limit $h \to 0$. The cusp is thus a finite ε–effect, and indeed moves to smaller h_c for decreasing ε (not shown). A further consequence, discussed in Fig.12 below, is that for finite ε, when varying h at $m = 0$ the T2 solutions must bifurcate from the T1 branch at $h = h_c$.

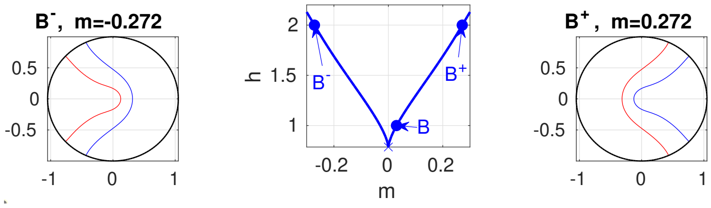

Figure 10: Continuation of the fold position m of the fold B from Fig.9 in height of cone h, $(a, \varepsilon) = (1.05, 0.15)$.

4.5. **Continuation in ε.** In Fig.11 we continue selected solutions from Fig.9 to smaller ε, aiming to verify that $E_\varepsilon(u_\varepsilon) \to |I_0|$ as $\varepsilon \to 0$. Decreasing ε is numerically challenging as it requires repeated and strong mesh refinement near the interface. In the BD in (a) we show E_ε over ε for the continuation of the T2 sample A from Fig.9 (orange branch), and for the T1 sample C from Fig.9 (blue branch). The blue branch (straight interface along the short semi-axis of length 1) should limit to $2\sqrt{2} \approx 2.82$ (independent of a), and $E_\varepsilon(u_\varepsilon)$ initially strongly increases and reaches $E_\varepsilon(u_\varepsilon) \approx 2.795$ at $\varepsilon = 0.025$. However the numerics become increasingly harder at small ε, and we stop at $\varepsilon = 0.025$, where we have adaptively refined from $n_t \approx 6000$ (at $\varepsilon = 0.15$) to $n_t \approx 60000$ triangles in the FEM mesh.

Note that, as observed in [Ton05], the minimizing interfaces in dimension 2 cannot have self-intersections. This does not contradict Figure 11 (b), since the illustrated interfaces are critical points but not minimizers.

For $a = 1$, the orange branch should limit to $E_0 \approx 2.71$, see Fig.5(a). This will not change significantly for small $a - 1 > 0$ as the interface is close to the short semi-axis of length 1 (see also Fig. 12 below for general dependence of branches on a), and with the refinement to $n_t \approx 35000$ in A at $\varepsilon = 0.025$ we believe that

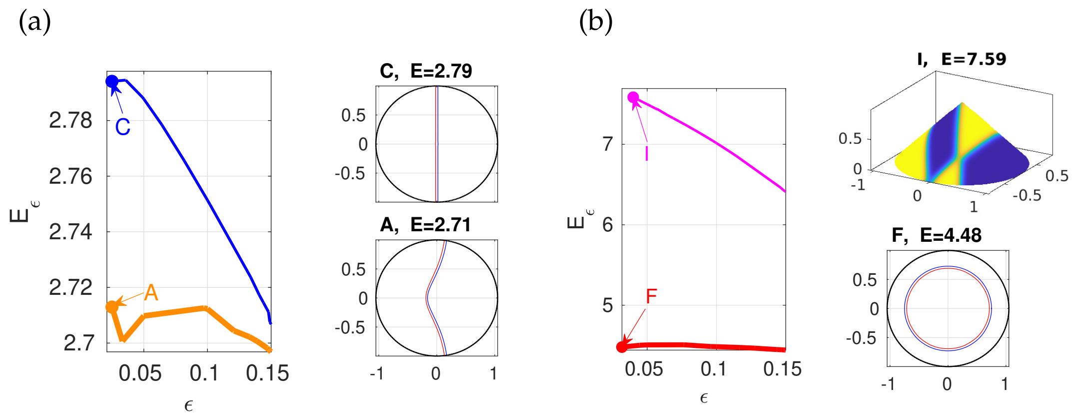

Figure 11: (a) Continuation in ε of the T2 (orange branch) and T1 (blue branch) solutions at $m = 0$ from Fig.9(a_2). (b) same for solutions F and I from Fig.9.

we obtain a good approximation of $l_2(h)$. The sample plots show the expected behavior of the solutions, i.e., the interfaces (of width ε) steepen up and hence the $u = \pm 0.5$ level lines in the samples move closer together. In (b), sample F shows the continuation of F from Fig.9 to $\varepsilon = 0.04$, and I the analogue for I from Fig.9, illustrating the two 4–end points 'expected' (see Remark 4.4b)) in the limit $\varepsilon \to 0$.

Remark 4.4. a) Theorem 1.2 does *not* apply to the blue branch, but down to $\varepsilon = 0.025$ the numerics suggest the convergence of u_ε to the tip–interface I_0, see also Remark 1.3(b) and the discussion after Fig.1. However, for smaller ε it becomes difficult to maintain the orientation of the interface in C, i.e., depending on the mesh small rotations of the interface may set in, and thus we stop the continuation. In any case, *if* we assume the convergence of $u_\varepsilon \to u_0$ for $\varepsilon \to 0$, then the blue branch shows that the convergence is *slower* than for branches (such as T2 and T3) on which interfaces avoid the tip. Moreover, this effect becomes stronger for more pointed cones, see Fig. 12(c), where we discuss the behavior of the T1 interface in dependence of ε in more detail for a cone of height $h = 3$.

b) We also have no proof of convergence for the interfaces on the magenta branch containing I, which again contains a straight segment through the tip. Other "higher order branches" with solutions with several phase domains but for which the interfaces avoid the tip show a better convergence behavior, similar to the branches containing A and F. ⌋

4.6. **Continuation in** h **and** a**, and again in** ε**.** In Fig.12 we aim to study the dependence of the three main types of solutions on a and h. We initially fix the "intermediate" $\varepsilon = 0.1$, and in (a) we restart similar to Fig.9 with the continuation in m at $h = 0.25$. As expected from Fig.10, the primary bifurcating branch b1 (blue) then goes horizontally through $m = 0$ with a T1 type solution at $m = 0$, i.e., the loop containing B and C in Fig.9(a_2) no longer exists.

In (b) we then continue samples A and B from (a) in h. For the T3 (red) branch, the energy E_ε compares reasonably well with the length l_3 from Fig.5(a), where again we note that the deviation due to finite $\varepsilon = 0.1$ is larger than the

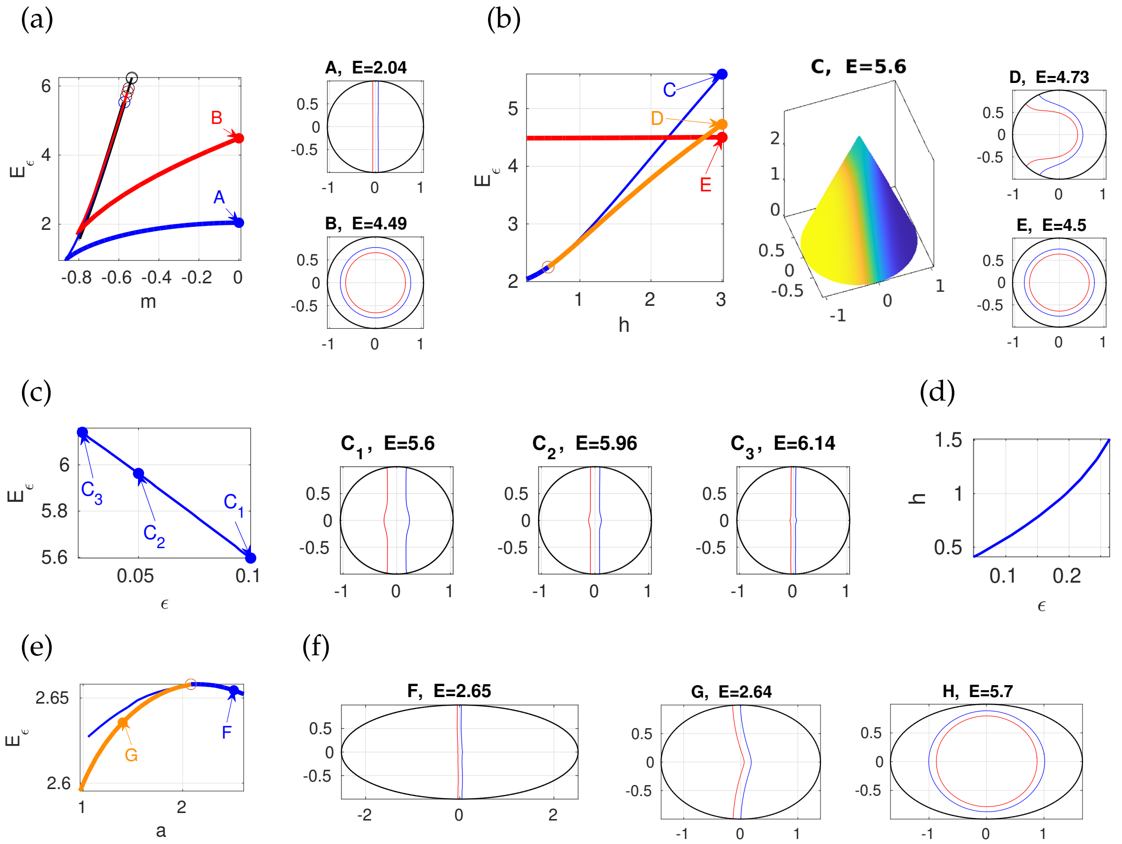

Figure 12: (a) T1 and T3 branches at $(h, a, \varepsilon) = (0.25, 1.05, 0.1)$. (b) Continuation of T1 and T3 at $m = 0$ from (a) in h. The T2 branch (magenta) bifurcates at $h = h_c =\approx 0.72$ from T1. The T3 solutions are global minima for $h \geq h_0 \approx 2.7$. (c) Continuation of C from (b) in ε, samples at $\varepsilon = 0.1$ (same as C), at $\varepsilon = 0.05$, and at $\varepsilon = 0.025$. (d) Branch point continuation of the BP at h_c from (b). (e,f) continuation of T1 from (b) at $h = 0.9$ in a. T2 reconnects to T_1 at $a = a_0 \approx 2.2$. The last plot in (d) also shows a continuation of T3 from (a) in a.

one due to $a - 1 = 0.05 > 0$. Namely, for the T3 branch E should not depend on h, and should be close to $\sqrt{2}\pi \approx 4.44$ (the limit $\varepsilon \to 0$ for $a = 1$), and this holds reasonably well. On the other hand, for the tip–interface branch branch T1 (blue) $E = 5.6$ in sample C at $h = 3$, while $l_1(3) = 2\sqrt{1+3^2} \approx 6.32$ (independent of a), i.e., the more pointed tip here induces a strong deviation even at relatively small $\varepsilon = 0.1$. Therefore, in (c) we continue C from (b) to smaller ε, where at $\varepsilon = 0.025$ in C_3 we have reached $E_\varepsilon = 6.14$. The contour plots in (c) show that for tip–interfaces the level lines $u = \pm\delta \neq 0$ (here $\delta = 0.5$) detour the tip for $\varepsilon > 0$, and this becomes more pronounced for more pointed cones (i.e., larger h, compare samples C,E in Fig.9 with $(h, \varepsilon) = (1, 0.15)$, C in Fig.11 with $(h, \varepsilon) = (1, 0.05)$, A in Fig.12(a) with $(h, \varepsilon) = (0.25, 0.1)$, and C_1 to C_3 with $h = 3$ and $\varepsilon = 0.1, 0.05, 0.025$). Thus, this effectively quantifies the effect of the strength of the conical singularity, yielding a slower convergence.

The most important difference between Fig.12(b) and Fig.5(a) is that the area–halving circular arc in Fig.5(a) exists for any $\alpha \in [0, 2\pi)$, and becomes straight for $\alpha = \dfrac{2\pi}{\sqrt{1+h^2}} \to 2\pi$, i.e., $h \to 0$. On the other hand, the T2 solutions in Fig. 12(b_2) with $\varepsilon = 0.1$ only exist for $h \geq h_c \approx 0.7$, where the (orange) T2 branch bifurcates from the T1 branch in a supercritical pitchfork. Again, this is due to the finite ε, and h_c decreases with ε: For $\varepsilon = 0.15$ we know from Fig.10 that the BP is given by the cusp of the fold point continuation and sits at $h \approx 0.8$, and in (d) we altogether show the BP location h over ε as obtained from branch point continuation [Uec21, §3.61.], where we need to stop near $\varepsilon = 0.04$ due to convergence problems.

Finally, in (e,f) we show the continuation of the T1 (blue) and T2 (orange) solutions from (b) at $h = 0.9$ in the ellipticity a.[5] For both, E only depends weakly on a; in fact, for T1 we should have $\lim_{\varepsilon\to 0} E_\varepsilon = 2\sqrt{1+0.9^2} \approx 2.69$ independent of a, but as in Fig.10 this requires extensive mesh-adaption, additional to the mesh–adaption already needed in Fig.12(d) for increasing a. Importantly, as we continue b1 we gain stability at a BP near $a = a_c \approx 2.2$, where the orange stable T2 branch bifurcates in a subcritical pitchfork. Alternatively, if we continue the T2 solution at $h = 0.9$ from (b) in a, then the obtained branch coincides with the orange branch in (e), and hence "reconnects" to the T1 branch at $a = a_c$. This intuitively makes sense as we expect the T2 solutions to approach the T1 solutions for large a, and the T1 solutions to become global minimizers. However, again this also depends on ε, and if we decrease ε the BP (or reconnection point) in (e) moves to larger a (not shown).

This, and further numerical experiments fully agree with Prop. 3.2, stating that tip interfaces are never minimizers at $\varepsilon = 0$: while for small $\varepsilon > 0$ and fixed $h > 0$, T1 interfaces are the global minimizers for sufficiently large a, for $\varepsilon \to 0$ at any fixed a they lose stability to the T2 interfaces.

A. Appendix: Auxiliary aspects of geometric measure theory

A.1. **Functions of bounded variation and the co-area formula.** Functions of bounded variation are suitable for the study of our Γ–convergence. They are defined on so-called *good* metric measure spaces, and there are two different gradient norms that can both be put into relation. With both gradient norms and the Hausdorff measure, one can define the perimeter and establish the co-area formula. Our main sources are [Vol10, Mir03, Nic11, FR60].

A.1.1. *Metric measure spaces and Hausdorff measure.*

Definition A.1. *Let $(X, \mathfrak{d}, \mu)$ be a metric measure space with metric $\mathfrak{d}$ and measure μ. It is called* good *if $(X, \mathfrak{d})$ is complete, and $(X, \mathfrak{d}, \mu)$ is doubling, i.e. if $B_R(x)$ denotes a ball in X of radius R centered at x, then there exists a uniform constant $c > 0$ such that*

[5] We also continue the T3 solutions, but for these E increases rather quickly from 4.5 and the branch cannot be plotted reasonably together with the T1 and T2 branches; hence we only give the sample H at $a \approx 1.7$, with $E \approx 5.7$.

for any $x \in X$ *and any* $R > 0$

$$\mu(B_{2R}(x)) \leq c \cdot \mu(B_R(x)).$$

A central example of such a good metric measure space in our context is a compact Riemannian manifold. The Riemannian metric defines the distance $\mathfrak{d}_g$ and the Riemannian Lebesgue measure $dvol_g$. Then $(M, \mathfrak{d}_g, dvol_g)$ is a good metric measure space in the sense of the definition above. More generally, compact manifolds with boundary and conical singularities, see Definition B.1, are good metric measure spaces. More generally, compact stratified spaces yield good metric measure spaces.

Definition A.2 (Hausdorff measure)**.**
Let $(X, \mathfrak{d}, \mu)$ *be a metric measure space. For any subset* $\Omega \subset X$*, any* $s \in [0, \infty)$ *define the* s*-dimensional Hausdorff measure*

$$\mathcal{H}^s_{\mathfrak{d}}(\Omega) := \sup_{\delta>0} \left[\inf \left\{ \frac{\pi^{s/2}}{\Gamma(3/2)} \sum_{j=1}^{\infty} \left(\frac{diam_{\mathfrak{d}}\Omega_j}{2} \right)^s : \Omega \subset \bigcup_{j=1}^{\infty} \Omega_j;\ diam_{\mathfrak{d}}\Omega_j \leq \delta \right\} \right],$$

where $diam_{\mathfrak{d}}\Omega_j$ *is the diameter of the smallest metric ball containing* Ω_j*, and* $\Gamma(s)$ *is the Gamma-function.*

The constant $\frac{\pi^{s/2}}{\Gamma(3/2)}$ ensures that the Hausdorff measure corresponds to the Lebesgue measure on smooth Riemannian manifolds (M, g) if $s = \dim M$. In that case, the Hausdorff measure $\mathcal{H}^s_g(\Omega)$ coincides with the Riemannian measure of a Borel set $\Omega \subset M$, cf. e.g. [Vol10, Theorem 2.17].

A.1.2. *Functions of bounded variation.*

Definition A.3 (Gradient for locally Lipschitz functions)**.**
Let $(X, \mathfrak{d}, \mu)$ *be a metric measure space. For any open* $\Omega \subset X$ *consider the space* $Lip_{loc}(\Omega)$ *of locally Lipschitz functions* $u : \Omega \to \mathbb{R}$*. For such* u *and any* $x \in X$ *we define*

$$\|\nabla u\|(x) := \liminf_{\rho \to 0} \left[\sup_{y \in \overline{B_\rho(x)}} \frac{|u(x) - u(y)|}{\rho} \right].$$

One can define the gradient norm for locally integrable functions $L^1_{\mathrm{loc}}(\Omega)$ on some open Ω.

Definition A.4 (Gradient of locally integrable functions)**.** *Let* $(X, \mathfrak{d}, \mu)$ *be a metric measure space. Let* $\Omega \subset X$ *be open and bounded, and* $u \in L^1_{loc}(\Omega)$*. Then*

$$\|\nabla u\|(\Omega) := \inf \left\{ \liminf_{n\to\infty} \int_\Omega \|\nabla u_n\|(x)\, d\mu(x) : (u_n)_n \subset Lip_{loc}(\Omega); u_n \xrightarrow{L^1_{loc}(\Omega)} u \right\}$$

Now, we can define functions of (locally) bounded variation.

Definition A.5. *The space of functions with (locally) bounded total variation is*

- $BV(\Omega) := \{u \in L^1_{loc}(\Omega) : \|\nabla u\|(\Omega) < \infty\}$
- $BV_{loc}(\Omega) := \{u \in L^1_{loc}(\Omega) : \|\nabla u\|(A) < \infty$ *for any* $A \subset \Omega$ *open,* $\overline{A} \subset \Omega$ *compact* $\}$

The gradient can be computed as a limit for an approximating sequence.

Proposition A.6 (Approximating $\|\nabla u\|(\Omega)$)**.** *For any* $u \in BV(\Omega)$ *with* $\|\nabla u\|(\Omega) < \infty$ *there exists* $(u_n) \subset Lip_{loc}(\Omega)$ *such that*

- $u_n \longrightarrow u$ *in* $L^1_{loc}(\Omega)$*,*
- $\|\nabla u\|(\Omega) = \lim_{n\to\infty} \int_\Omega \|\nabla u_n\|(x) = \lim_{n\to\infty} \|\nabla u_n\|(\Omega).$

Proof. The statement can be found in [Mir03, p. 984]. □

We will also need the following result.

Theorem A.7 (lower semi-continuity)**.** *Suppose* $(u_n) \subset BV(\Omega)$*, and we have convergence* $u_n \longrightarrow u$ *in* $L^1_{loc}(\Omega)$ *as* $n \to \infty$*. Then*

$$\|\nabla u\|_g(\Omega) \leq \liminf_{n\to\infty} \|\nabla u_n\|_g(\Omega). \tag{A.1}$$

The proof of Theorem A.7, see e.g. [Vol10, Theorem 2.38], does not require any conditions on Ω. In particular $\overline{\Omega} \subset M$ does not need to be compact.

We conclude the section with a definition of perimeter.

Definition A.8 (Caccioppoli sets)**.** *Let* $(X, \mathfrak{d}, \mu)$ *be a good metric measure space, arising from a Riemannian manifold* (M, g) *of dimension* d*. Let* $E \subset M$ *be a* $\mathcal{H}^d_\mathfrak{d}$*-measurable set. The perimeter of* E *in* M *is defined by*

$$P_g(E, \Omega) := \|\nabla \chi_E\|(\Omega),$$

where $\chi_E : M \to \{0, 1\}$ *is the characteristic function of* E*. If the perimeter is finite,* E *is called a Caccioppoli set with respect to* Ω*.*

This definition is compatible with our intuitive understanding of the perimeter as the (Hausdorff) measure of the boundary. Namely, by e.g., [Giu84, Ch. 1], if $E \subset M$ is a Borel set with C^1-boundary ∂E, then E is a Caccioppoli set with

$$P_g(E, M) = \mathcal{H}^{d-1}_\mathfrak{d}(\partial E). \tag{A.2}$$

A.2. **Γ-convergence.** Γ-convergence is a powerful tool from the calculus of variations in order to study convergence of minimizers. We will recall the most important definitions and properties of Γ-convergence based on [Rin18, Ch. 13.1].

Definition A.9 (Abstract Γ-Convergence). *Let X be a complete metric space. The functional $\mathcal{F}_\infty : X \to \mathbb{R} \cup \{+\infty\}$ is called (sequential) Γ-limit of the functionals $\mathcal{F}_k : X \to \mathbb{R} \cup \{+\infty\}$ (denoted by $\mathcal{F}_\infty := \Gamma - \lim_{k\to\infty} \mathcal{F}_k$), $k \in \mathbb{N}$, if the following two conditions are satisfied.*

- *For all sequences $(u_k) \subset X$ the " $\liminf$-inequality" holds*

$$u = \lim_{k\to\infty} u_k \quad \Longrightarrow \quad \mathcal{F}_\infty[u] \le \liminf_{k\to\infty} \mathcal{F}_k[u_k] \tag{A.3}$$

- *For all $u \in X$ there exists as **recovery sequence** $(u_k) \subset X$ such that*

$$u = \lim_{k\to\infty} u_k, \quad \mathcal{F}_\infty[u] = \lim_{k\to\infty} \mathcal{F}_k[u_k]. \tag{A.4}$$

Remark A.10. *If the first condition in Definition A.9 is satisfied, then the second condition can be altered to the so called " $\limsup$-inequality": For all $u \in X$ there exists a sequence $u_k \longrightarrow u$ in X as $k \to \infty$ such that*

$$\mathcal{F}_\infty[u] \ge \limsup_{k\to\infty} \mathcal{F}_k[u_k]. \tag{A.5}$$

An important consequence of Γ-convergence is that the limit functional $\mathcal{F}_\infty = \Gamma - \lim_{k\to\infty} \mathcal{F}_k$ is lower semi-continuous, cf. [Rin18, Proposition 13.2]. Moreover, Γ-convergence implies convergence of minima and the corresponding minimizers. More specifically we have the following results.

Theorem A.11. *Let X be a complete metric space. Consider a sequence of functionals $\mathcal{F}_k : X \to \mathbb{R} \cup \{+\infty\}$, $k \in \mathbb{N}$, and assume that the Γ-limit $\mathcal{F}_\infty = \Gamma - \lim_{k\to\infty} \mathcal{F}_k$ exists.*

1. *Assume that the functionals $\{\mathcal{F}_k\}_{k\in\mathbb{N}}$ are equicoercive, i.e. there exists a compact set $K \subset X$ such that $\inf_X \mathcal{F}_k = \inf_K \mathcal{F}_k$ for all $k \in \mathbb{N}$. Then, $\mathcal{F}_\infty$ has a minimizer and*

$$\min_X \mathcal{F}_\infty = \lim_{k\to\infty} \inf_X \mathcal{F}_k.$$

   In addition, all accumulation points of any precompact sequence $(u_k) \subset X$ with the property $\liminf_{k\to+\infty} \mathcal{F}_k[u_k] = \liminf_{k\to+\infty} \inf_X \mathcal{F}_k$ are minimizers of $\mathcal{F}_\infty$.

2. *Without the assumption of equicoercivity, a minimizer for $\mathcal{F}_\infty$ need not exist a priori and we only have: If a sequence $\{u_k\} \subset X$ of minimizers for $\{\mathcal{F}_k\}$ converges to $u \in X$, then u is a minimizer of $\mathcal{F}_\infty$ and $\lim_{k\to.\infty} \mathcal{F}_k[u_k] = \mathcal{F}_\infty[u]$.*

Proof. See e.g. [Rin18, Theorem 13.3] for the first statement and [Mod87, Proposition 4] for the second statement. □

Remark A.12. As noted in Remark 1.3, for our problem we can establish $u_\varepsilon \to u_0$ in $L^1(M)$ via a priori estimates on u_ε in $H^1(M)$ and the compact embedding $H^1(M) \hookrightarrow L^1(M)$, which in fact yields the equicoercivity of our E_ε. ⌋

B. Conical singularities. $\mathcal{D}(\Delta_D), \mathcal{D}(\Delta_N)$ versus $H^2(M)$

Definition B.1. *A* compact manifold with boundary and conical singularity P *is a metric space* $\overline{M} = M \cup \{P\}$ *where* M*, the regular part, is a smooth manifold, equipped with a Riemannian metric* g*, which admits a decomposition*

$$M = \mathcal{C}(N) \cup_N X$$

into a compact Riemannian manifold X *with disjoint boundary components* N *and* ∂M *and an open truncated generalized cone* $\mathcal{C}(N)$ *over the closed manifold* N*. That is,* $\mathcal{C}(N) = (0,1] \times N$ *and the metric on* $\mathcal{C}(N)$ *takes the special 'conical' form*

$$g|_{\mathcal{C}(N)} := dr^2 \oplus r^2 g^N(r), \;\; r \in (0,1],$$

where $g^N(r)$ *is a family of metrics on* N *which is smooth up to* $r = 0$*. The boundary* $\{1\} \times N$ *of* $\mathcal{C}(N)$ *is glued to the boundary component* N *of* X*, and the metric on* $\overline{M}$ *is defined by using the metric* d_M *on* M *induced by* g *and setting, for* $Q \in M$*,*

$$d(P,Q) := \lim_{r \to 0} d_M((r,y),Q) \quad \textit{for any } y \in N.$$

This means that the cone tip $\{P\}$ corresponds to $r = 0$.[6] N is referred to as the *cross section* of the conical singularity. See Figure 13 for an example with $\partial M = \emptyset$. We also speak of M as a manifold with conical singularity P. In a similar way we can admit several (finitely many) conical singularities.

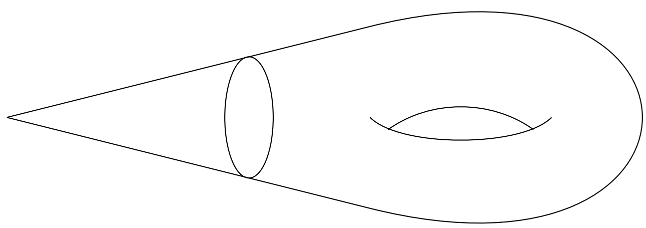

Figure 13: Illustration of a manifold with a conical singularity.

For a surface $\overline{M}$, where $N = \mathbb{S}^1$, we define the *angle* of the conical singularity as $\alpha = \lim_{r\to 0} \frac{\ell_r}{r}$ where ℓ_r is the length of $\mathbb{S}^1$ with respect to $g_{\mathbb{S}^1}(r)$. If $\overline{M}$ is a straight cone embedded in $\mathbb{R}^3$ with the conical tip at P (i.e. $\overline{M}$ is a union of

[6] See [Gri11] and [MW04] for more details on conical singularities, in particular for the proof that the intuitive notion of 'submanifold of $\mathbb{R}^m$ with conical singularity' satisfies this condition.

straight segments starting at P, then g_N is independent of r), then ℓ_r is the length of the intersection of $\overline{M}$ with a sphere of radius r around P, for small r. The angle α also defines the opening angle in a representation of $\overline{M}$ as a subset of the plane (see Figure 5(b)). For the elliptic cone (3.1) the intersection with a small sphere is a convex curve contained in the open lower half sphere, so $\alpha < 2\pi$.

We want to show here that for $\alpha > 2\pi$ in spite of (2.6) generally

$$\begin{aligned} \mathcal{D}(\Delta_D) &\supsetneqq \{u \in H^2(M) : \operatorname{tr} u = 0\}, \\ \mathcal{D}(\Delta_N) &\supsetneqq \{u \in H^2(M) : \operatorname{tr} \circ \partial_\nu u = 0\}. \end{aligned} \tag{B.1}$$

Let $(\lambda, \omega_\lambda)_\lambda$ be the set of eigenvalues and an orthonormal basis of corresponding eigenfunctions of the Laplace Beltrami operator Δ_N of $(N = \mathbb{S}^1, g_N)$. Consider the minimal and maximal domains $\mathcal{D}(\Delta_{\min}), \mathcal{D}(\Delta_{\max})$ of the Laplacian, defined exactly as in (2.1) with ∇ replaced by Δ. Classical arguments, see also e.g. some recent applications [MV12, Lemma 2.2] or [KLP08], show that for each $\omega \in \mathcal{D}(\Delta_{\max})$ there exist constants $c^\pm_\lambda(\omega)$ for all $\lambda \in [0,1)$, such that ω admits a partial asymptotic expansion as $r \to 0$

$$\begin{aligned} \omega = &\sum_{\lambda=0} (c^+_\lambda(\omega) + c^-_\lambda(\omega)\log(r)) \cdot \omega_\lambda \\ &+ \sum_{\lambda \in (0,1)} \left(c^+_\lambda(\omega) r^{\sqrt{\lambda}} + c^-_\lambda(\omega) r^{-\sqrt{\lambda}} \right) \cdot \omega_\lambda + \widetilde{\omega}, \end{aligned} \tag{B.2}$$

where $\widetilde{\omega} \in \mathcal{D}(\Delta_{\min})$. The domains $\mathcal{D}(\Delta_D), \mathcal{D}(\Delta_N)$ are characterized by conditions on the coefficients $c^\pm_\lambda(\omega)$ that replace the usual boundary conditions: $\omega \in \mathcal{D}(\Delta_{\max})$ is an element of $\mathcal{D}(\Delta_D)$ or $\mathcal{D}(\Delta_N)$ if and only if $c^-_\lambda(\omega) = 0$ for all λ, in addition to Dirichlet or Neumann boundary conditions at the regular boundary, respectively. We can now give an example for (B.1).

Example B.2. Consider the conical singularity $(r, \theta) \in (0,1] \times \mathbb{S}^1$ with metric $dr^2 + c^2 r^2 d\theta^2$, where $c > 1$ and hence angle $\alpha = 2\pi c > 2\pi$. Here $\dim M \equiv m = 2$. Then $(N, g_N) = (\mathbb{S}^1, c^2 d\theta^2)$ with eigenvalues λ given by $k^2/c^2, k \in \mathbb{Z}$. Consider a cutoff function $\phi \in C^\infty[0,1]$ with $\phi \equiv 1$ near $r = 0$ and $\phi \equiv 0$ near $r = 1$, and the first non zero eigenvalue $1/c^2$ with eigenfunction ω_{1/c^2}. Then $\omega(r, \theta) := r^{1/c}\omega_{1/c^2}(\theta)\phi(r)$ lies in $\mathcal{D}(\Delta_D)$ and $\mathcal{D}(\Delta_N)$. However, $\partial_r^2 \omega = r^{-2+1/c}\omega_{1/c^2}$ near $r = 0$, which is not in $L^2(M, g)$ since the volume element is $r\,dr d\theta$, and hence $\omega \notin H^2(M)$.

References

[BL92] J. Brüning and M. Lesch. *Hilbert complexes.* J. Funct. An., 108, pp. 88–132, 1992.

[BNAP22] V. Benci, S. Nardulli, L. Acevedo, and P. Piccione. *Lusternik-Schnirelman and Morse theory for the van der Waals–Cahn–Hilliard equa-*

tion with volume constraint. Nonlinear Anal., 220, Paper No. 112851, 29, 2022.

[Che83] J. Cheeger. *Spectral geometry of singular Riemannian spaces.* J. Differential Geom., 18 (4), pp. 575–657 (1984), 1983.

[CHL10] Xinfu Chen, D. Hilhorst, and E. Logak. *Mass conserving Allen-Cahn equation and volume preserving mean curvature flow.* Interfaces Free Bound., 12, 2010.

[CR71] M. G. Crandall and P. H. Rabinowitz. *Bifurcation from simple eigenvalues.* J. Funct. Anal., 8, pp. 321–340, 1971.

[DF20] Q. Du and X. Feng. *The phase field method for geometric moving interfaces and their numerical approximations.* In Handbook of Num. Anal., vol. 21, pages 425–508. Elsevier, 2020.

[Ell89] C. M. Elliott. *The Cahn-Hilliard model for the kinetics of phase separation.* In Math. models for phase change problems (Óbidos, 1988), vol. 88 of Internat. Ser. Numer. Math., pp. 35–73. Birkhäuser, Basel, 1989.

[ESS92] L. C. Evans, H. M. Soner, and P. E. Souganidis. *Phase transitions and generalized motion by mean curvature.* Comm. Pure Appl. Math., 45(9), pp. 1097–1123, 1992.

[Eva98] L.C. Evans. *Partial Differential Equations.* AMS, 1998.

[Fed14] H. Federer. *Geometric measure theory.* Springer, 2014.

[FR60] W. Fleming and R. Rishel. *An Integral Formula for Total Gradient Variation.* Archiv Math., 11 (1), pp. 218–222, 1960.

[GG18] P. Gaspar and M. Guaraco. *The Allen–Cahn equation on closed manifolds.* Calc. Var. PDE. 57 (4), pp. 1–42, 2018.

[GHP03] C. E. Garza-Hume and P. Padilla. *Closed geodesics on oval surfaces and pattern formation.* Comm. Anal. Geom., 11 (2), pp. 223–233, 2003.

[Giu84] E. Giusti. *Minimal Surfaces and Functions of Bounded Variation.* Monographs in Math. 80. 1984.

[GM88] M. E. Gurtin and H. Matano. *On the structure of equilibrium phase transitions within the gradient theory of fluids.* Quart. Appl. Math., 46(2), pp. 301–317, 1988.

[Gri11] D. Grieser. *A natural differential operator on conic spaces.* Discrete Contin. Dyn. Syst., Dynamical systems, Diff. Eq. and Appl. 8th AIMS Conference. Suppl. Vol. I, pp. 568–577, 2011.

[GS02] M. Golubitsky and I. Stewart. *The symmetry perspective.* Birkhäuser, Basel, 2002.

[Hoy06] R.B. Hoyle. *Pattern formation.* Cambridge Univ. Press., 2006.

[HT00] J. Hutchinson and Y. Tonegawa. *Convergence of phase interfaces in the van der Waals-Cahn-Hilliard theory.* Calc. Var. PDE., 10 (1), pp. 49–84, 2000.

[KLP08] K. Kirsten, P. Loya, and J. Park. *Functional determinants for general self-adjoint extensions of Laplace-type operators resulting from the generalized cone.* Manuscripta Math., 125 (1), pp. 95–126, 2008.

[KLPW15] M. Kowalczyk, Yong Liu, F. Pacard, and Juncheng Wei. *End-to-end construction for the Allen-Cahn equation in the plane.* Calc. Var. PDE., 52 (1-2), pp. 281–302, 2015.

[Kuz04] Y. A. Kuznetsov. *Elements of applied bifurcation theory.* Springer, 3d edition, 2004.

[LP61] G. Lumer and R.S. Phillips. *Dissipative operators in a Banach space.* Pacific J. Math., (11) 1961.

[Lun95] A. Lunardi. *Analytic semigroups and optimal regularity in parabolic problems.* Birkhäuser, Basel, 1995.

[Mir03] M. Miranda. *Functions of bounded variation on "good" metric spaces.* J. Math. Pures Appl. 82 (8), pp. 975–1004, 2003.

[Mir19] A. Miranville. *The Cahn-Hilliard equation, volume 95 of CBMS-NSF Regional Conference Series in Applied Mathematics.* SIAM, PA, Recent advances and appl., 2019.

[Mod87] L. Modica. *The Gradient Theory of Phase Transitions and the Minimal Interface Criterion.* Arch. Rat. Mech. and Anal., 98 (2), pp. 123–142, 1987.

[Mor16] F. Morgan. *Geometric measure theory: a beginner's guide.* Acad. Press, 2016.

[MV12] R. Mazzeo and B. Vertman. *Analytic Torsion on Manifolds with Edges.* Adv. in Math., 231 (2), pp. 1000–1040, 2012.

[MW04] R. Melrose and J. Wunsch. *Propagation of singularities for the wave equation on conic manifolds.* Invent. Math., 156 (2), pp. 235–299, 2004.

[Nic11] L. Nicolaescu. *The Co-area Formula.* available at www3.nd.edu/ lnicolae/Coarea.pdf, 2011.

[Pac12] F. Pacard. *The role of minimal surfaces in the study of the Allen-Cahn equation.* In Geometric analysis, Partial Differential Equations and surfaces, vol. 570 of Contemp. Math., pp. 137–163. Amer. Math. Soc., Providence, RI, 2012.

[Rin18] F. Rindler. *Calculus of Variations.* Springer, 2018.

[RS13] N. Roidos and E. Schrohe. *The Cahn-Hilliard equation and the Allen-Cahn equation on manifolds with conical singularities.* Comm PDE, 38 (5), pp. 925–943, 2013.

[Ton05] Y. Tonegawa. *On stable critical points for a singular perturbation problem.* Comm. Anal. Geom., 13 (2), pp. 439–459, 2005.

[Uec21] H. Uecker. *Numerical Continuation and Bifurcation in Nonlinear PDEs.* SIAM, Philadelphia, PA, 2021.

[Uec23a] H. Uecker. *Continuation of fold points, branch points, and Hopf points with constraints in pde2path.* available at [Uec23b], 2023.

[Uec23b] H. Uecker. available online at www.staff.uni-oldenburg.de/hannes.uecker/pde2path, 2023.

[Ver16] B. Vertman. *The biharmonic heat operator on edge manifolds and nonlinear fourth order equations.* Manuscripta Math, (146), pp. 179–203, 2016.

[Vol10] A. Volkmann. *Regularity of isoperimetric hypersurfaces with obstacles in Riemannian manifolds.* Diplomarbeit, Albert-Ludwigs-Universität Freiburg, 2010.

* daniel.grieser@uni-oldenburg.de, University Oldenburg, Germany
† sina.held@uni-oldenburg.de, University Oldenburg, Germany
‡ hannes.uecker@uni-oldenburg.de, University Oldenburg, Germany
♯ boris.vertman@uni-oldenburg.de University Oldenburg, Germany